



Non-local Thermodynamic Equilibrium Abundance Analyses of the Extreme Helium Stars V652 Her and HD 144941

Gajendra Pandey¹ and David L. Lambert² ¹ Indian Institute of Astrophysics; Bangalore, 560034, India; pandey@iiap.res.in² The W.J. McDonald Observatory and Department of Astronomy, University of Texas at Austin; Austin, TX 78712-1083, USA; dll@astro.as.utexas.edu

Received 2017 June 5; revised 2017 August 24; accepted 2017 August 24; published 2017 September 29

Abstract

Optical high-resolution spectra of V652 Her and HD 144941, the two extreme helium stars with exceptionally low C/He ratios, have been subjected to a non-LTE abundance analysis using the tools TLUSTY and SYNSPEC. Defining atmospheric parameters were obtained from a grid of non-LTE atmospheres and a variety of spectroscopic indicators including He I and He II line profiles, and the ionization equilibrium of ion pairs such as C II/C III and N II/N III. The various indicators provide a consistent set of atmospheric parameters: $T_{\text{eff}} = 25,000 \pm 300$ K, $\log g = 3.10 \pm 0.12$ (cgs), and $\xi = 13 \pm 2$ km s⁻¹ are provided for V652 Her, and $T_{\text{eff}} = 22,000 \pm 600$ K, $\log g = 3.45 \pm 0.15$ (cgs), and $\xi = 10$ km s⁻¹ are provided for HD 144941. In contrast to the non-LTE analyses, the LTE analyses—LTE atmospheres and an LTE line analysis—with the available indicators do not provide a consistent set of atmospheric parameters. The principal non-LTE effect on the elemental abundances is on the neon abundance. It is generally considered that these extreme helium stars with their very low C/He ratio result from the merger of two helium white dwarfs. Indeed, the derived composition of V652 Her is in excellent agreement with predictions by Zhang & Jeffery, who model the slow merger of helium white dwarfs; a slow merger results in the merged star having the composition of the accreted white dwarf. In the case of HD 144941, which appears to have evolved from metal-poor stars, a slow merger is incompatible with the observed composition but variations of the merger rate may account for the observed composition. More detailed theoretical studies of the merger of a pair of helium white dwarfs are to be encouraged.

Key words: stars: abundances – stars: atmospheres – stars: chemically peculiar – stars: evolution – stars: fundamental parameters

Supporting material: machine-readable tables

1. Introduction

Extreme helium stars (EHes) are very hydrogen-poor stars with effective temperatures of about 10,000–30,000 K (i.e., spectral types A and B) with surface gravities of $\log g \sim 1$ for the coolest stars and increasing to ~ 3 for the hottest stars. The majority of EHes populate a locus of roughly constant $\log L/M \sim 4.5$, where the luminosity L and mass M are in solar units. This locus most likely represents an evolutionary track with stars evolving at about constant luminosity from low to high temperatures. Such EHes, thought to form from the merger of a helium white dwarf with a carbon–oxygen white dwarf, have carbon-to-helium ratios by number of about 0.6%, with presently analyzed stars exhibiting C/He ratios by number in the range 0.3%–1.0%. The carbon is provided by the surface of the C–O white dwarf, and the helium primarily by the helium white dwarf.

At the time of Jeffery’s (2008) succinct review of EHes, about 20 Galactic EHes were known. Two are set apart from the majority highlighted above by a much lower C/He ratio. According to Jeffery et al. (2001) and an LTE analysis, V652 Her has a low C/He ratio of 0.006%; according to Harrison & Jeffery’s (1997) LTE abundance analysis, HD 144941 has an even lower C/He ratio of 0.0017%. Both ratios are sharply lower than the C/He ratio of the majority of the EHes. In addition, V652 Her and HD 144941 have higher surface gravities than the majority of EHes with the same effective temperature and thus correspond to a $\log L/M$ smaller than the majority by about a factor of 1.3 dex. These differences, especially the low C/He ratio, suggest a different origin,

namely the merger of a helium white dwarf with another helium white dwarf (see again the review in Jeffery (2008) for further details).

In this paper, we describe a non-LTE analysis of new high-quality optical spectra of both V652 Her and HD 144941 primarily in order to determine how non-LTE effects influence the C/He ratio, but also to measure the effects of departures from LTE on the abundances of other elements. The paper follows our similar analyses of non-LTE effects on several EHes having C/He ratios characteristic of the majority of EHes (Pandey & Lambert 2011; Pandey et al. 2014).

2. Observations

High-resolution optical spectra of V652 Her and HD 144941 were obtained on 2011 May 13 at the coudé focus of the W.J. McDonald Observatory’s Harlan J. Smith 2.7 m telescope with the Robert G. Tull cross-dispersed échelle spectrograph (Tull et al. 1995) at a resolving power of $R = 60,000$. Three thirty-minute exposures were recorded for each of these stars. The observing procedure and the wavelength coverage is the same as described in Pandey et al. (2001). The Image Reduction and Analysis Facility software package was used to reduce these recorded spectra. HD 144941’s spectrum, obtained from the Anglo-Australian Telescope (AAT) and analyzed by Przybilla et al. (2005), was made available by S. Jeffery (2017, private communication) for comparison.

The sample wavelength interval shown in Figure 1 displays the extracted spectrum from each exposure of the observed EHes. All of the spectra were aligned to the rest wavelengths of

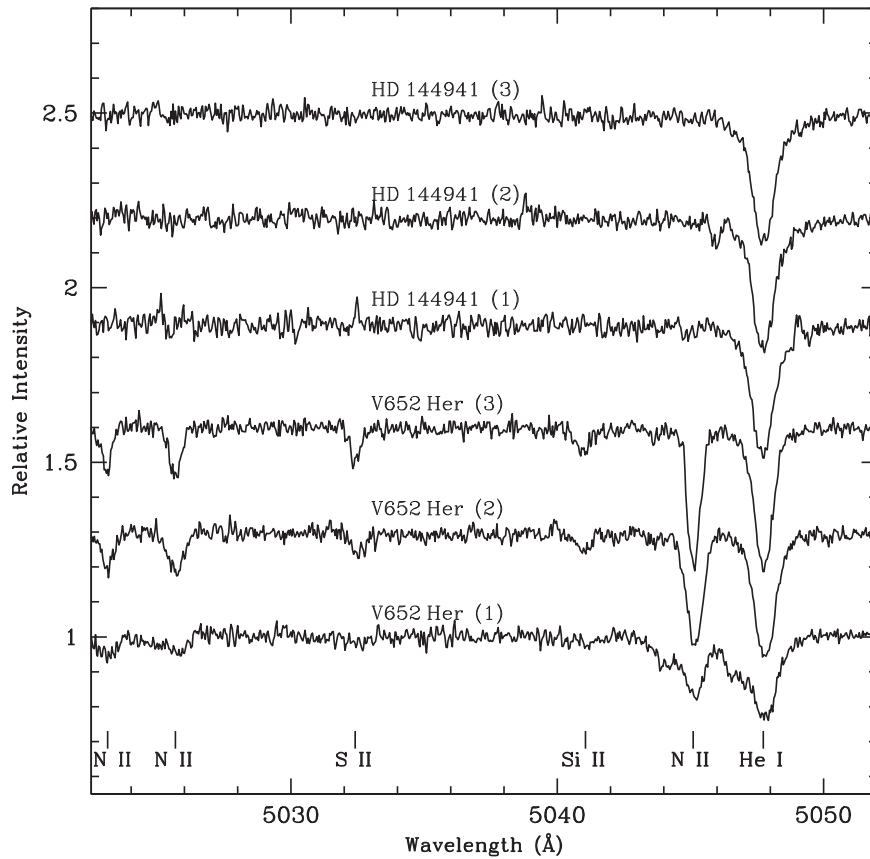


Figure 1. A sample spectral region is shown for three exposures each of V652 Her and HD 144941. The exposure numbers are given in parentheses, and the positions of the key lines are identified in this window from 5023 to 5052 Å.

Table 1
Summary of Atmospheric Parameters

Star	Analyses	T_{eff} (K)	$\log g$ (cgs units)	ξ (km s^{-1})	$v \sin i$ (km s^{-1})
V652 Her	non-LTE	$25,000 \pm 300$	3.10 ± 0.12	13 ± 2	10–12
V652 Her	LTE	$25,300 \pm 300$	3.25 ± 0.12	13 ± 2	10–12
HD 144941	non-LTE	$22,000 \pm 600$	3.45 ± 0.15	10	10
HD 144941	LTE	$21,000 \pm 600$	3.35 ± 0.15	10	10

well-known lines. Inspection of Figure 1 shows that the line profiles are not always symmetric. Note the obvious asymmetry in the two exposures of V652 Her, attributable to atmospheric pulsations (Jeffery et al. 2001). V652 Her pulsates with a period of 2.592 hr (Landolt 1975) and a radial velocity amplitude of about 70 km s^{-1} (Hill et al. 1981). For the abundance analysis, we have used the spectrum of V652 Her, showing symmetric profiles with a signal-to-noise ratio of about 140 per pixel at 5600 Å. The line profiles of HD 144941 for each exposure appear symmetric and show extremely weak metal lines. Therefore, these exposures were coadded to enhance the signal-to-noise ratio for the abundance analyses; the signal-to-noise ratio is about 280 per pixel at 5600 Å.

The pure absorption line spectrum of V652 Her is dominated by contributions from the following species: H I, He I, N II, N III, O II, Ne I, Al III, Si II, Si III, S II, S III, and Fe III. However, the absorption line spectrum of HD 144941 is dominated by H I, and He I lines and a small collection of weak lines from other species. The Revised Multiplet Table (Moore 1972), tables of spectra of H, C, N, and O (Moore 1993), and the *NIST*

Atomic Spectra Database³ (version 5.3) were used for line identification.

The primary objective is to determine reliable atmospheric parameters (effective temperature, surface gravity and microturbulence) and then the chemical composition of V652 Her and HD 144941.

3. Quantitative Fine Analyses

Non-LTE line-blanketed model atmospheres are used to determine atmospheric parameters and chemical composition. The effective temperature T_{eff} and surface gravity g are obtained from intersecting loci in the T_{eff} versus $\log g$ plane. These loci represent the ionization equilibrium of available ion pairs such as C II/C III, N II/N III, Si II/Si III, Si III/Si IV, and S II/S III, and loci derived from the best fits to the Stark-broadened profiles of He I and He II lines. The microturbulent velocity ξ is obtained from both the N II and the O II lines, with each ion providing lines spanning a range in equivalent width.

³ <http://www.nist.gov/pml/data/asd.cfm>

Table 2
Measured Equivalent Widths (W_λ) and NLTE/LTE Photospheric Line Abundances for V652 Her

Line	χ (eV)	$\log gf$	W_λ (mÅ)	$\log \epsilon(X)$	
				NLTE ^a	LTE ^b
H I λ 4101.734	10.199	-0.753	Synth	9.42	9.65
H I λ 4340.462	10.199	-0.447	Synth	9.47	9.64
H I λ 4861.323	10.199	-0.020	Synth	9.52	9.69
Mean	9.47 ± 0.05	9.66 ± 0.03
C II λ 3920.681*	16.333	-0.232	35	7.21	6.94
C II λ 4267.001*	18.046	+0.563
C II λ 4267.183*	18.046	+0.716
C II λ 4267.261*	18.046	-0.584	125	7.29	6.94
C II λ 6578.050*	14.449	-0.026	69	7.04	6.86
C II λ 6582.880*	14.449	-0.327	45	7.08	6.90
Mean	7.16 ± 0.12	6.91 ± 0.04
C III λ 4647.418*	29.535	+0.070	25	6.86	6.88
C III λ 4650.246*	29.535	-0.151	22	6.92	7.02
Mean	6.90 ± 0.04	6.95 ± 0.10
N II λ 3955.851*	18.466	-0.849	139	...	8.56
N II λ 3994.997*	18.497	+0.163	308	8.75	8.99
N II λ 4227.736*	21.600	-0.061	153	...	8.64
N II λ 4459.937*	20.646	-1.476	28	8.77	8.63
N II λ 4507.560*	20.666	-0.817	74	...	8.54
N II λ 4564.760*	20.409	-1.589	30	...	8.73
N II λ 4601.478*	18.466	-0.452	220	8.73	8.87
N II λ 4607.153*	18.462	-0.522	206	8.73	8.83
N II λ 4613.868*	18.466	-0.665	194	8.79	8.86
N II λ 4621.393*	18.466	-0.538	215	8.79	8.91
N II λ 4630.539*	18.483	+0.080	316	8.78	...
N II λ 4643.086*	18.483	-0.371	222	8.55	8.82
N II λ 4654.531*	18.497	-1.506	85	...	8.83
N II λ 4667.208*	18.497	-1.646	65	...	8.79
N II λ 4674.908*	18.497	-1.553	80	...	8.84
N II λ 4718.377	27.746	-0.042	33	...	8.91
N II λ 4774.244*	20.646	-1.280	51	...	8.78
N II λ 4779.722*	20.646	-0.587	106	...	8.60
N II λ 4781.190*	20.654	-1.337	40	...	8.70
N II λ 4788.138*	20.654	-0.363	120	...	8.49
N II λ 4803.287*	20.666	-0.113	160	...	8.57
N II λ 4810.299*	20.666	-1.084	54	...	8.63
N II λ 4987.376*	20.940	-0.584	87	...	8.53
N II λ 4991.243*	25.491	-0.180	50	...	8.81
N II λ 4997.224*	25.491	-0.657	28	...	8.96
N II λ 5002.703*	18.462	-1.022	126	...	8.65
N II λ 5023.053*	25.507	-0.165	60	...	8.91
N II λ 5045.099*	18.483	-0.407	245	8.66	8.83
N II λ 5073.592*	18.497	-1.550	85	...	8.91
N II λ 5179.344	27.980	+0.497
N II λ 5179.521	27.746	+0.675	95	...	8.71
N II λ 5183.200	27.980	-0.090	26	...	8.94
N II λ 5184.961	27.739	-0.044	26	...	8.84
N II λ 5452.070*	21.148	-0.881	60	8.74	8.66
N II λ 5454.215*	21.153	-0.782	97	8.88	8.91
N II λ 5478.086*	21.153	-0.930	40	...	8.47
N II λ 5480.050*	21.160	-0.711	56	...	8.45
N II λ 5495.655*	21.160	-0.220	106	...	8.43
N II λ 5526.234*	25.491	-0.312	45	8.58	8.93
N II λ 5530.242*	25.498	+0.113	81	8.48	8.90
N II λ 5535.347*	25.507	+0.398
N II λ 5535.383*	25.491	-0.204	135	8.43	8.98
N II λ 5540.061*	25.491	-0.557	32	8.65	8.98
N II λ 5543.471*	25.498	-0.092	68	8.59	8.98
N II λ 5551.922*	25.507	-0.189	63	8.64	9.03
N II λ 5676.020*	18.462	-0.367	236	8.77	9.06
N II λ 5710.770*	18.483	-0.518	199	8.87	8.88
N II λ 5730.660*	18.483	-1.703	51	...	8.77
N II λ 5747.300*	18.497	-1.091	116	...	8.77

Table 2
(Continued)

Line	χ (eV)	$\log gf$	W_λ (mÅ)	$\log \epsilon(X)$	
				NLTE ^a	LTE ^b
N II λ 5767.450*	18.497	-1.447	95	...	8.95
N II λ 6136.890*	23.132	-1.124	23	...	8.89
N II λ 6150.750*	23.125	-1.086	24	...	8.87
N II λ 6167.750*	23.142	+0.025	122	...	8.86
N II λ 6170.160*	23.125	-0.311	73	...	8.75
N II λ 6173.310*	23.132	-0.126	100	...	8.82
N II λ 6340.580*	23.246	-0.192	79	...	8.73
N II λ 6346.860*	23.239	-0.901	37	...	8.96
N II λ 6379.620*	18.466	-1.191	103	8.60	8.81
N II λ 6482.050*	18.497	-0.311	229	8.82	9.04
N II λ 6504.610*	23.246	-0.626	55	...	8.93
Mean	8.70 \pm 0.12	8.80 \pm 0.16
N III λ 4514.850*	35.671	+0.221	46	...	9.13
N III λ 4634.130*	30.459	-0.086	78	8.52	8.81
N III λ 4640.640*	30.463	+0.168	100	8.41	8.81
Mean	8.50 \pm 0.10	8.92 \pm 0.18
O II λ 4345.560*	22.979	-0.346	62	7.64	7.67
O II λ 4366.895*	22.999	-0.348	60	7.60	7.64
O II λ 4414.899*	23.441	+0.172	104	7.53	7.64
O II λ 4416.975*	23.419	-0.077	107	7.78	7.91
O II λ 4452.378*	23.442	-0.788	23	7.56	7.65
O II λ 4590.974*	25.661	+0.350	70	7.79	7.68
O II λ 4596.177*	25.661	+0.200	52	7.72	7.63
O II λ 4638.856*	22.966	-0.332	64	7.64	7.69
O II λ 4649.135*	22.999	+0.308	140	7.64	7.74
O II λ 4650.838*	22.966	-0.362	38	7.35	7.40
O II λ 4661.632*	22.979	-0.278	62	7.57	7.62
O II λ 4676.235*	22.999	-0.394	42	7.44	7.50
O II λ 4699.011*	28.510	+0.418
O II λ 4699.218*	26.225	+0.270	36	7.37	7.30
O II λ 4705.346*	26.249	+0.477	44	7.43	7.40
O II λ 5206.651*	26.561	-0.266	15	7.73	7.69
Mean	7.59 \pm 0.14	7.61 \pm 0.15
Ne I λ 5852.488*	16.848	-0.490	20	...	8.51
Ne I λ 6143.063*	16.619	-0.100	53	8.13	8.62
Ne I λ 6163.594*	16.715	-0.620	24	7.98	8.72
Ne I λ 6266.495*	16.715	-0.370	25	7.75	8.50
Ne I λ 6334.428*	16.619	-0.320	40	8.23	8.69
Ne I λ 6382.991*	16.671	-0.240	40	8.13	8.62
Ne I λ 6402.246*	16.619	+0.330	104	8.09	8.72
Ne I λ 6506.528*	16.671	-0.030	52	8.07	8.58
Ne I λ 6598.953*	16.848	-0.360	22	7.97	8.48
Ne I λ 7032.413*	16.619	-0.260	40	8.16	8.67
Mean	8.06 \pm 0.14	8.61 \pm 0.09
Mg II λ 4481.126*	8.864	+0.749
Mg II λ 4481.150*	8.864	-0.553
Mg II λ 4481.325*	8.864	+0.594	211	7.09	7.48
Al III λ 4149.913	20.555	+0.620
Al III λ 4149.968	20.555	-0.680
Al III λ 4150.173	20.555	+0.470	103	...	6.40
Al III λ 4479.885	20.781	+0.900 ^c
Al III λ 4479.971	20.781	+1.020 ^c
Al III λ 4480.009	20.781	-0.530 ^c	75	...	5.93
Al III λ 4512.565	17.808	+0.410	89	...	6.24
Al III λ 4528.945	17.818	-0.290
Al III λ 4529.189	17.818	+0.660	146	...	6.34
Al III λ 5696.604	15.642	+0.230	169	...	6.67
Al III λ 5722.730	15.642	-0.070	126	...	6.60
Mean	6.36 \pm 0.27
Si II λ 4128.054	9.837	+0.359	30	...	7.19
Si II λ 4130.872	9.839	-0.783
Si II λ 4130.894	9.839	+0.552	34	...	7.04
Si II λ 5041.024	10.066	+0.029	35	...	7.67

Table 2
(Continued)

Line	χ (eV)	$\log gf$	W_λ (mÅ)	$\log \epsilon(X)$	
				NLTE ^a	LTE ^b
Si II $\lambda 5055.984$	10.074	+0.523	44	...	7.30
Mean	7.30 \pm 0.27
Si III $\lambda 3796.124^*$	21.730	+0.407
Si III $\lambda 3796.203^*$	21.730	-0.703	167	7.18	7.04
Si III $\lambda 3806.526^*$	21.739	+0.679
Si III $\lambda 3806.700^*$	21.739	-0.071	307	7.60	7.69
Si III $\lambda 4567.840^*$	19.016	+0.068	285	7.40	7.85
Si III $\lambda 4574.757^*$	19.016	-0.409	204	7.34	7.57
Si III $\lambda 4716.654^*$	25.334	+0.491	83	7.46	7.15
Si III $\lambda 4813.333^*$	25.979	+0.708	85	7.04	7.11
Si III $\lambda 4819.712^*$	25.982	+0.937
Si III $\lambda 4819.814^*$	25.982	-0.354	116	7.01	7.24
Si III $\lambda 4828.951^*$	25.987	+0.937
Si III $\lambda 4829.111^*$	25.980	-0.354	120	7.03	7.16
Si III $\lambda 5739.734^*$	19.722	-0.096	226	7.36	7.76
Mean	7.27 \pm 0.21	7.40 \pm 0.32
Si IV $\lambda 4088.862^*$	24.050	+0.194	185	7.63	7.75
Si IV $\lambda 4116.104^*$	24.050	-0.110	120	7.48	7.44
Mean	7.56 \pm 0.11	7.60 \pm 0.22
P III $\lambda 4222.198$	14.610	+0.210	80	...	5.42
P III $\lambda 4246.720$	14.610	-0.120	65	...	5.61
Mean	5.52 \pm 0.13
S II $\lambda 5032.434$	13.672	+0.188	40	...	7.35
S II $\lambda 5103.332$	13.672	-0.457	25	...	7.76
S II $\lambda 5212.620$	15.068	+0.316	25	7.21	7.33
S II $\lambda 5320.723$	15.068	+0.431	27	7.12	7.26
S II $\lambda 5428.655^*$	13.584	-0.177	20	7.57	7.37
S II $\lambda 5432.797^*$	13.617	+0.205	35	7.46	7.27
S II $\lambda 5509.705^*$	13.617	-0.175	20	7.56	7.37
S II $\lambda 5564.958$	13.672	-0.336	33	...	7.80
S II $\lambda 5606.151$	13.733	+0.124	25	...	7.22
S II $\lambda 5639.977$	14.067	+0.258
S II $\lambda 5640.346$	13.701	-0.036	45	...	7.23
S II $\lambda 5660.001$	13.677	-0.222	17	...	7.37
Mean	7.38 \pm 0.21	7.39 \pm 0.20
S III $\lambda 4253.589^*$	18.244	+0.107	174	7.46	7.18
S III $\lambda 4284.979^*$	18.193	-0.233	103	7.28	6.90
S III $\lambda 4332.692^*$	18.188	-0.564	66	7.26	6.88
S III $\lambda 4354.566^*$	18.311	-0.959	53	7.49	7.15
S III $\lambda 4361.527^*$	18.244	-0.606	68	7.32	6.95
S III $\lambda 4364.747^*$	18.318	-0.805	34	7.07	6.74
S III $\lambda 4499.245^*$	18.294	-1.640	16	7.52	7.20
Mean	7.34 \pm 0.16	7.00 \pm 0.18
Ar II $\lambda 4806.021$	16.644	+0.210	32	...	6.91
Fe III $\lambda 4137.764$	20.613	+0.630 ^c	42	6.74	7.05
Fe III $\lambda 4164.731$	20.634	+0.923 ^c	83	6.91	7.20
Fe III $\lambda 4296.851$	22.860	+0.418 ^c
Fe III $\lambda 4296.851$	22.860	+0.879 ^c	30	6.71	7.02
Fe III $\lambda 4310.355$	22.869	+0.189 ^c
Fe III $\lambda 4310.355$	22.869	+1.156 ^c	45	6.76	7.05
Fe III $\lambda 4395.755$	8.256	-2.595 ^c	39	7.04	7.34
Fe III $\lambda 4419.596$	8.241	-2.218 ^c	81	7.15	7.38
Fe III $\lambda 4431.019$	8.248	-2.572 ^c	38	7.02	7.30
Fe III $\lambda 5063.421$	8.648	-2.950 ^c	18	7.14	7.42
Fe III $\lambda 5086.701$	8.659	-2.590 ^c	40	7.17	7.46
Fe III $\lambda 5127.387$	8.659	-2.218 ^c	100	...	7.66
Fe III $\lambda 5156.111$	8.641	-2.018 ^c	100	7.31	7.46
Fe III $\lambda 5235.658$	18.266	-0.107 ^c	33	...	7.18
Fe III $\lambda 5243.306$	18.270	+0.405 ^c	71	...	7.13
Fe III $\lambda 5276.476$	18.264	-0.001 ^c	36	...	7.13
Fe III $\lambda 5282.297$	18.266	+0.108 ^c	43	...	7.12
Fe III $\lambda 5299.926$	18.261	-0.166 ^c	31	...	7.21
Fe III $\lambda 5302.602$	18.262	-0.120 ^c	31	...	7.17

Table 2
(Continued)

Line	χ (eV)	$\log gf$	W_λ (mÅ)	$\log \epsilon(X)$	
				NLTE ^a	LTE ^b
Fe III λ 5460.799	14.178	-1.519 ^c	30	6.88	7.59
Fe III λ 5485.517	14.176	-1.469 ^c	30	6.83	7.54
Fe III λ 5573.424	14.175	-1.390 ^c	42	6.92	7.64
Fe III λ 5833.938	18.509	+0.616 ^c	66	...	6.96
Fe III λ 5891.904	18.509	+0.498 ^c	54	...	6.96
Fe III λ 5929.685	18.509	+0.351 ^c	48	...	7.04
Mean	7.05 \pm 0.16	7.30 \pm 0.22

Notes. ^aLines covered by the adopted model atom, including the extended model atom with more levels, for the ions providing the ionization balance and some other ions.

^a (T_{eff} , $\log g$, ξ) = (25,000, 3.10, 13.0).

^b (T_{eff} , $\log g$, ξ) = (25,300, 3.25, 13.0).

^c Kurucz gf -value.

(This table is available in machine-readable form.)

In principle, the chemical composition of the adopted model atmosphere must match the composition derived from a spectrum. This match is achieved iteratively. Note that model atmospheres computed with C/He of 0.003%–0.03% and H/He of 0.0001 and 0.1 have the same atmospheric structure and so provide the same atmospheric parameters, including the composition. This helpful aide to the abundance analysis arises because neutral He is the dominant opacity source for the two EHes.

Since the photoionization of neutral helium is the main source of continuous opacity, lines of another species, say C II, are sensitive to the C/He abundance ratio. Abundances are given as $\log \epsilon(X)$ and normalized with respect to $\log \sum \mu_X \epsilon(X) = 12.15$, where μ_X is the atomic weight of element X. Since all of the elements except He have a very low abundance, the logarithmic He abundance is 11.54.

Our abundance analyses were carried out with non-LTE model atmospheres and non-LTE (and LTE) line formation for all major elements. For a few minor elements, the abundance analysis could be done only in LTE. Partially line-blanketed non-LTE model atmospheres were computed with the code TLUSTY (Hubeny 1988; Hubeny & Lanz 1995) using atomic data and model atoms provided on the TLUSTY home page,⁴ as described in Pandey et al. (2014). These model atmospheres included opacity from both bound-free and bound-bound transitions of H, He, C, N, O, Ne, Mg, Si, S, and Fe in non-LTE. The adopted model atoms, with their number of levels given in parentheses, are: H I(9), He I(14), He II(14), C I(8), C II(11), C III(12), C IV(13), N I(13), N II(6), N III(11), N IV(12), O I(22), O II(29), O III(29), Ne I(35), Ne II(32), Ne III(34), Mg II(14), Si II(16), Si III(12), Si IV(13), S II(14), S III(20), Fe II(36), and Fe III(50). Of the model atoms available in TLUSTY, these choices each refer to the smallest of the available atoms for many ions. Use of these model atoms suffices for the calculations of model atmospheres but, as we describe below, larger model atoms are used for the calculations of equivalent widths of lines.

Model atmospheres in LTE were also computed using TLUSTY. Model grids in non-LTE and LTE were computed covering the ranges $T_{\text{eff}} = 20,000$ (1000) 30,000 K and $\log g = 3.0$ (0.1) 4.5 cgs.

In this paper, we have used TLUSTY and SYNSPEC for calculating LTE and non-LTE model atmospheres and line profiles (Hubeny 1988; Hubeny et al. 1994; Hubeny & Lanz 1995, 2011, 2017). The stellar atmospheric parameters provided in Table 1 are determined from the spectra of V652 Her and HD 144941 on the assumption of both non-LTE and LTE using the lines given in Tables 2 and 3. Except where noted, the gf -values of the lines are taken from the NIST database⁵ (version 5.3). A few other sources consulted for gf -values are given in footnotes to the relevant tables.

TLUSTY model atmospheres are calculated with line opacity provided by the smallest of the available model atoms for many ions, as detailed above. In many cases, the observed lines are not contained within these model atoms. In order to extend the non-NLTE calculations to more of the observed lines, we ran the statistical equilibrium calculations with larger model atoms available in TLUSTY as described in Hubeny & Lanz (2017). Results are provided for the following model atoms: C II(22), C III(23), N II(42), N III(32), O II(29), Ne I(35), and Si III(30). Lines with both the upper and lower level within the model atom are marked by * in Tables 2 and 3. We note that our non-LTE abundance analysis using model atmospheres with extended (more levels) model atoms is fairly consistent in terms of the ionization balance and the derived abundances when compared with the analysis using small (fewer levels) model atoms; the mean abundances differ by about 0.05 to 0.3 dex, and individual line abundances differ by typically ≤ 0.3 dex. However, for most of the ions, we notice that the larger model atoms provide relatively less line-to-line scatter in the derived abundances.

For the elements H to Fe, the identification of lines suitable for analysis is not a major issue for V652 Her. In particular, a good selection of clean lines representing the ions of key elements is available. For HD 144941, lines of H, He, N, and O are available in good number, but fewer lines are present for C, Ne, Al, Si, and S, with Fe represented only by upper limits to equivalent widths of the most promising lines of Fe III. Moore (1993) is the primary source of wavelengths and classifications for these lines.

⁴ <http://nova.astro.umd.edu/index.html>

⁵ <http://www.nist.gov/pml/data/asd.cfm>

Table 3
Measured Equivalent Widths (W_λ) and NLTE/LTE Photospheric Line Abundances for HD 144941

Line	χ (eV)	$\log gf$	W_λ (mÅ)	$\log \epsilon(X)$	
				NLTE ^a	LTE ^b
H I λ 4101.734	10.199	-0.753	Synth	10.47	10.41
H I λ 4340.462	10.199	-0.447	Synth	10.32	10.32
H I λ 4861.323	10.199	-0.020	Synth	10.24	10.19
Mean	10.37 \pm 0.09	10.35 \pm 0.05
C II λ 6578.050*	14.449	-0.026	88	6.88	6.64
C II λ 6582.880*	14.449	-0.327	52	6.84	6.58
Mean	6.86 \pm 0.03	6.61 \pm 0.04
N II λ 3994.997*	18.497	+0.163	74	6.68	6.98
N II λ 4447.030*	20.409	+0.221	22	6.50	6.72
N II λ 4601.478*	18.466	-0.452	16	6.49	6.75
N II λ 4607.153*	18.462	-0.522	15	6.54	6.80
N II λ 4621.393*	18.466	-0.538	15	6.54	6.81
N II λ 4630.539*	18.483	+0.080	35	6.36	6.64
N II λ 4994.360*	25.498	-0.164
N II λ 4994.370*	20.940	-0.098	8	6.55	6.75
N II λ 5001.474*	20.654	+0.435	24	6.47	6.69
N II λ 5025.659*	20.666	-0.558	8	6.94	7.15
N II λ 5045.099*	18.483	-0.407	16	6.49	6.76
N II λ 5666.630*	18.466	-0.080	12	6.10	6.37
N II λ 5676.020*	18.462	-0.367	8	6.19	6.47
N II λ 5679.560*	18.483	+0.250	24	6.11	6.39
N II λ 6482.050*	18.497	-0.311	7	6.17	6.45
Mean	6.44 \pm 0.23	6.70 \pm 0.22
O II λ 4414.899*	23.441	+0.172	19	6.94	6.87
O II λ 4416.975*	23.419	-0.077	16	7.10	7.02
O II λ 4590.974*	25.661	+0.350	14	7.24	7.10
O II λ 4596.177*	25.661	+0.200	11	7.26	7.12
O II λ 4638.856*	22.966	-0.332	8	6.94	6.86
O II λ 4649.135*	22.999	+0.308	37	7.15	7.08
O II λ 4650.838*	22.966	-0.362	7	6.91	6.83
Mean	7.08 \pm 0.15	6.98 \pm 0.13
Ne I λ 6143.063*	16.619	-0.100	12	7.26	7.49
Ne I λ 6402.246*	16.619	+0.330	28	7.26	7.50
Ne I λ 6506.528*	16.671	-0.030	10	7.14	7.38
Mean	7.22 \pm 0.07	7.46 \pm 0.07
Mg II λ 4481.126*	8.864	+0.749
Mg II λ 4481.150*	8.864	-0.553
Mg II λ 4481.325*	8.864	+0.594	51	5.77	5.88
Al III λ 4479.885	20.781	+0.900 ^c
Al III λ 4479.971	20.781	+1.020 ^c
Al III λ 4480.009	20.781	-0.530 ^c	20	...	5.11
Al III λ 4512.565	17.808	+0.410	21	...	5.22
Al III λ 4528.945	17.818	-0.290
Al III λ 4529.189	17.818	+0.660	33	...	5.17
Al III λ 5696.604	15.642	+0.230	21	...	4.96
Al III λ 5722.730	15.642	-0.070	11	...	4.95
Mean	5.08 \pm 0.12
Si II λ 5041.024	10.066	+0.029	8	...	6.11
Si II λ 5055.984	10.074	+0.523	15	...	5.90
Mean	6.01 \pm 0.15
Si III λ 4552.622*	19.016	+0.292	70	6.11	5.93
Si III λ 4567.840*	19.016	+0.068	46	6.03	5.85
Si III λ 4574.757*	19.016	-0.409	20	6.01	5.84
Si III λ 4819.712*	25.982	+0.937
Si III λ 4819.814*	25.982	-0.354	12	5.75	5.99
Si III λ 4828.951*	25.987	+0.937
Si III λ 4829.111*	25.980	-0.354	16	5.90	6.15
Si III λ 5739.734*	19.722	-0.096	23	6.16	5.95
Mean	5.99 \pm 0.15	5.95 \pm 0.11
S II λ 5432.797*	13.617	+0.205	12	6.08	6.09
S III λ 4253.589*	18.244	+0.107	30	6.30	5.71
S III λ 4284.979*	18.193	-0.233	17	6.31	6.11
S III λ 4332.692*	18.188	-0.564	\leq 15	\leq 6.59	\leq 6.39

Table 3
(Continued)

Line	χ (eV)	$\log gf$	W_λ (mÅ)	$\log \epsilon(X)$	
				NLTE ^a	LTE ^b
Mean	6.31 ± 0.01	5.91 ± 0.28
Fe III λ 4395.755	8.256	-2.595 ^c	≤ 19	≤ 7.09	≤ 6.79
Fe III λ 4419.596	8.241	-2.218 ^c	≤ 29	≤ 6.96	≤ 6.62
Fe III λ 4431.019	8.248	-2.572 ^c	≤ 16	≤ 6.99	≤ 6.68
Fe III λ 5127.387	8.659	-2.218 ^c	≤ 20	≤ 6.98	≤ 6.59
Fe III λ 5156.111	8.641	-2.018 ^c	≤ 14	≤ 6.60	≤ 6.21
Mean	$\leq 6.60 \pm 0.00$	$\leq 6.21 \pm 0.00$

Notes. ^aLines covered by the adopted model atom, including the extended model atom with more levels, for the ions providing the ionization balance and some other ions.

^a ($T_{\text{eff}}, \log g, \xi$) = (22,000, 3.45, 10.0).

^b ($T_{\text{eff}}, \log g, \xi$) = (21,000, 3.35, 10.0).

^c Kurucz gf -value.

(This table is available in machine-readable form.)

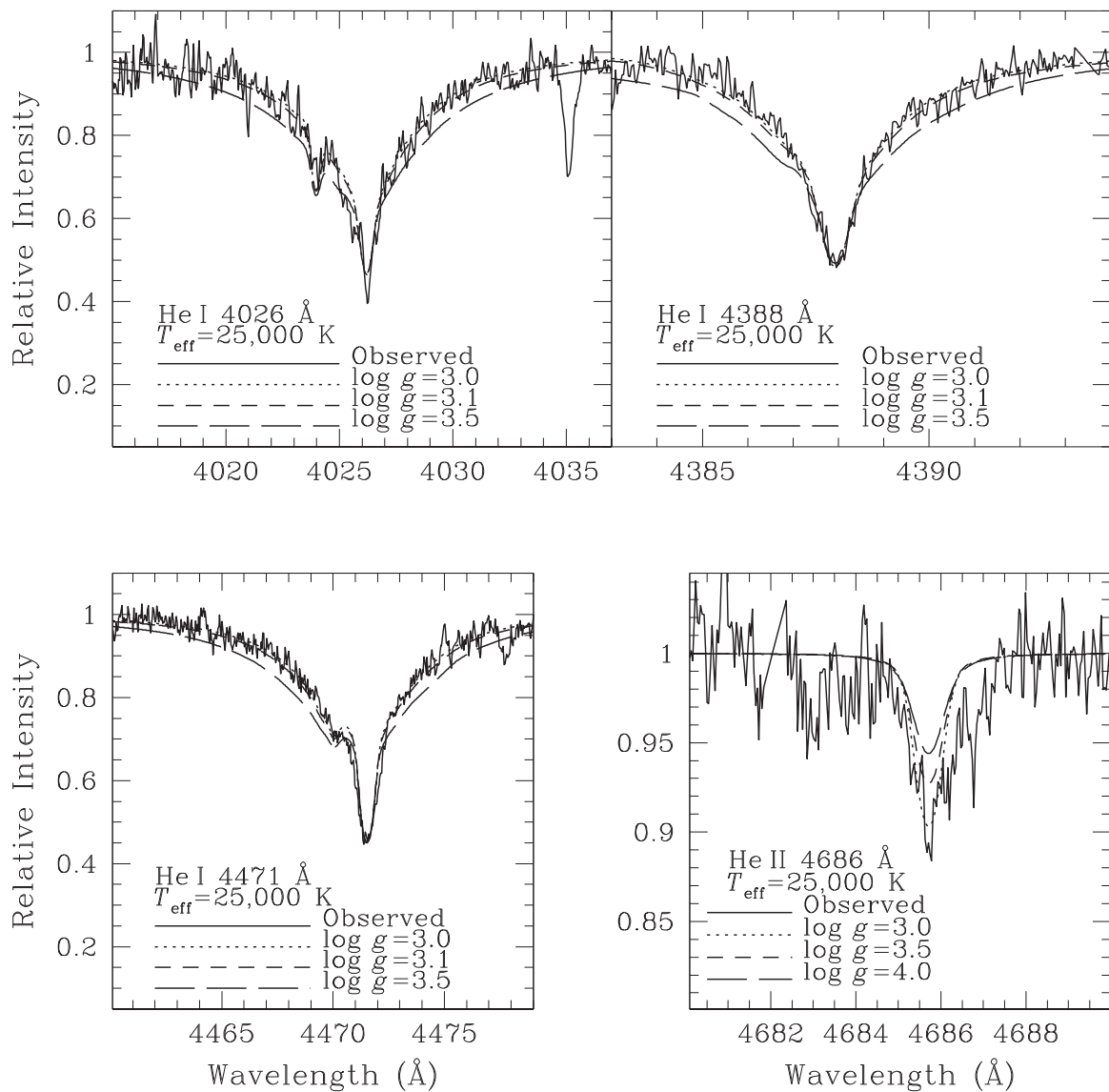


Figure 2. Observed spectrum of V652 Her and theoretical NLTE He I and He II line profiles calculated using the NLTE model $T_{\text{eff}} = 25,000$ K for three different $\log g$ values—see the key on the figure.

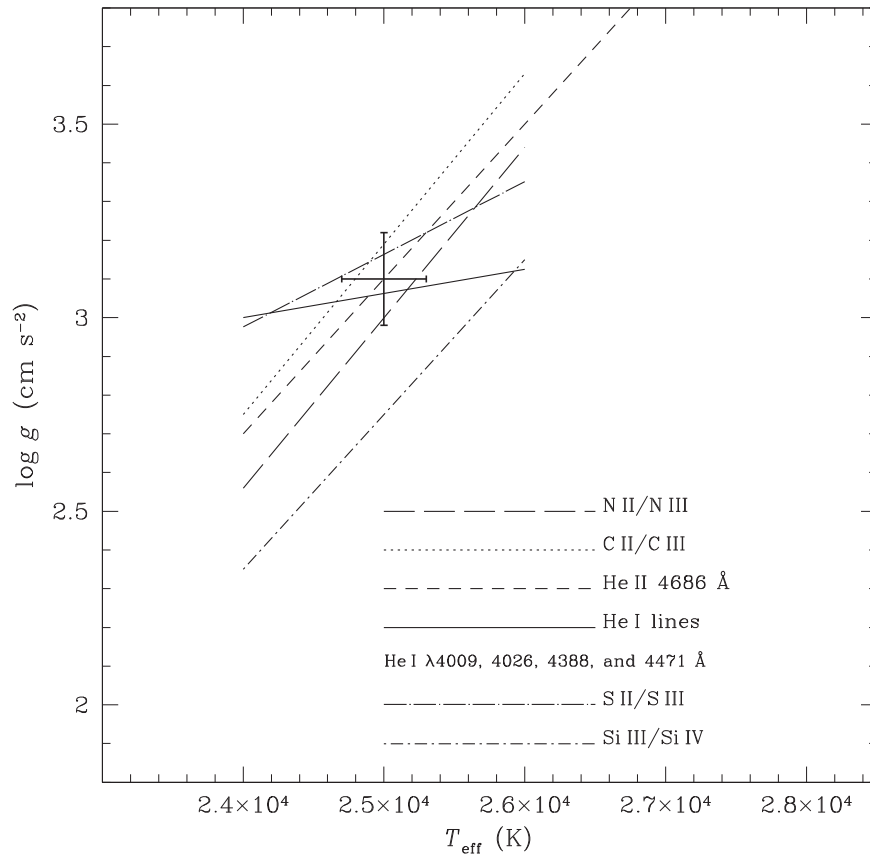


Figure 3. T_{eff} vs. $\log g$ plane for V652 Her. Loci satisfying ionization equilibria are plotted—see the keys on the figure. The loci satisfying optical He I and He II line profiles are shown. The cross shows the adopted NLTE model atmosphere parameters.

3.1. V652 Her

3.1.1. Non-LTE Analyses

The non-LTE code SYNSPEC (Hubeny et al. 1994) was adopted to compute the line profiles and the theoretical equivalent widths using the non-LTE model atmospheres. The observed absorption profile or its measured equivalent width was matched with the SYNSPEC prediction to obtain the non-LTE abundance. The unresolved blends of two or more lines were dealt with by synthesizing them and then matching them to the observed feature by adjustment of abundances.

For determining the T_{eff} , $\log g$, and ξ , a standard procedure was followed. The microturbulent velocity ξ was estimated from N II and O II lines as they show a wide range in equivalent width. To minimize the temperature dependence, N II lines with similar lower excitation potentials (LEP) were used: N II lines were used with LEPs about 18, 21, 23, and 25 eV. ξ was found from the requirement that the derived abundance is independent of the measured equivalent width. A microturbulent velocity $\xi = 13 \pm 2 \text{ km s}^{-1}$ was obtained from N II and O II lines.

Ionization equilibrium was imposed, using model atmospheres computed with small model atoms, to provide loci in the (T_{eff} , $\log g$) plane for the following pairs of ions: C II/C III, N II/N III, S II/S III, and Si III/Si IV; however, low weight was given to the last ratio because the Si abundances from the Si III lines show a large line-to-line scatter.

Fits to the Stark-broadened wings of the He I and He II line profiles provide additional loci in the (T_{eff} , $\log g$) plane. The

line broadening coefficients are from TLUSTY/SYNSPEC, which adopts the line broadening coefficients for He I 4471, 4388, and 4026 Å from Barnard et al. (1974) and Shamey (1969). For He I 4009 Å, TLUSTY/SYNSPEC uses an approximate Stark broadening treatment. For He II 4686 Å, TLUSTY/SYNSPEC uses a broadening table from Schoening (I. Hubeny 2017, private communication). The predicted line profiles depend on the electron densities and, therefore, on the temperature and surface gravity. Observed profiles of the He I 4471, 4388, 4026, and 4009 Å lines, and the He II 4686 Å, were used in the analysis.

Sample observed profiles of the He I and He II 4686 Å line are shown in Figure 2 with predicted non-LTE profiles for a non-LTE atmosphere of $T_{\text{eff}} = 25,000 \text{ K}$ and three different surface gravities. The He I and He II loci were obtained by fitting the line profiles for a range of effective temperatures. Note that the predicted profiles have been convolved with the instrumental profile and the stellar rotation profile. A projected rotation velocity of 10–12 km s^{-1} was obtained from fits of synthetic spectra to clean O II lines with an allowance for the instrumental profile.

The loci derived from the application of ionization equilibrium to C, N, Si, and S ions are also added to the loci from the He I and He II profiles. Figure 3 shows these loci. Their intersection suggests that the best non-LTE model atmosphere has $T_{\text{eff}} = 25,000 \pm 300 \text{ K}$ and $\log g = 3.10 \pm 0.12$.

HI observed profiles at 4102, 4340, and 4861 Å were chosen for estimating the non-LTE hydrogen abundance by spectrum

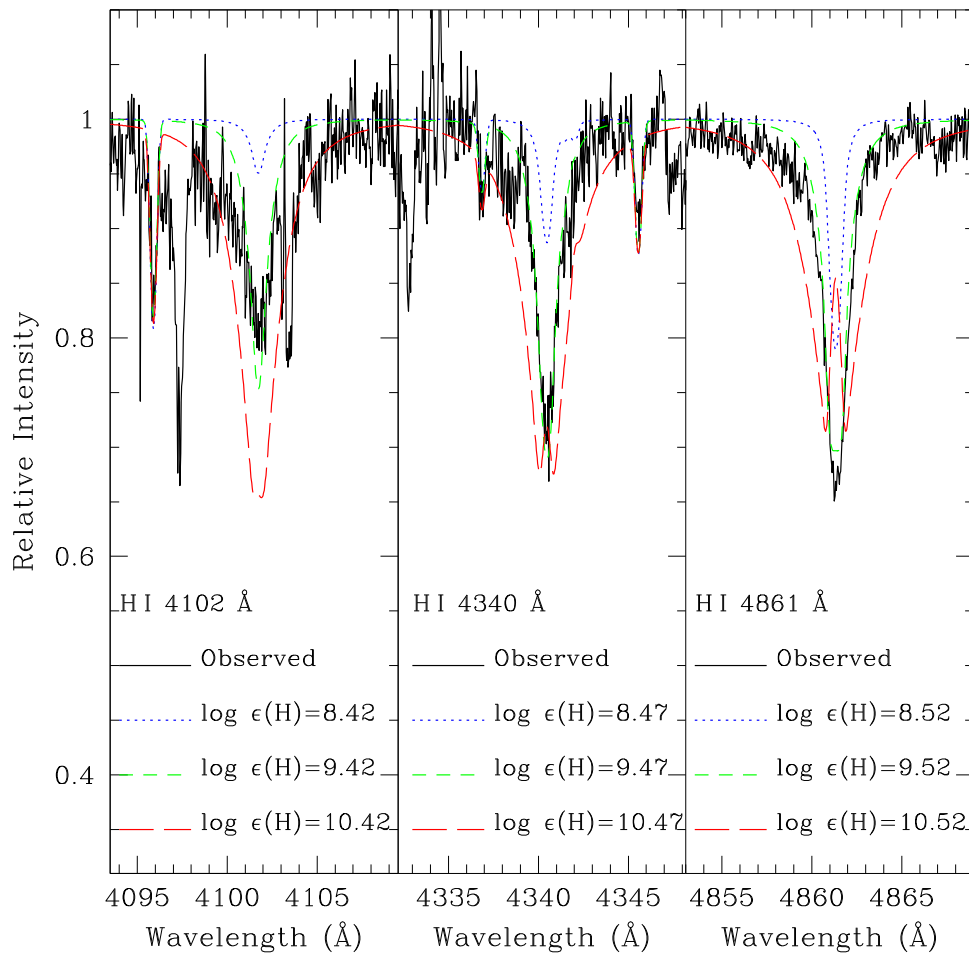


Figure 4. Observed spectrum of V652 Her and theoretical NLTE H I line profiles calculated using the NLTE model $T_{\text{eff}} = 25,000$ K and $\log g = 3.1$ for three different H abundances—see the key on the figure.

synthesis. The line wings of the 4340 and 4861 Å profiles are used mainly for this purpose. It is noted that the best-fitting theoretical profile for each line does not have an emission core, but such cores appear for theoretical profiles of higher H abundance. Less weight is given to the NLTE hydrogen abundance derived from the poor signal-to-noise profile of 4102 Å line. The hydrogen model atoms and the line broadening coefficients adopted from Vidal et al. (1973) are from TLUSTY. Observed profiles of the 4102, 4340, and 4861 Å are shown in Figure 4, with predicted non-LTE profiles for a non-LTE atmosphere of $T_{\text{eff}} = 25,000$ K and $\log g = 3.10$ for three different hydrogen abundances.

The abundances of all of the elements were derived for the adopted model atmosphere ($T_{\text{eff}}, \log g, \xi$) = (25,000, 3.10, 13.0), computed with extended model atoms. The final photospheric line-by-line non-LTE abundances, including the mean abundance and the line-to-line scatter, are given in Table 2. The abundance rms errors due to uncertainty in T_{eff} and $\log g$, from C II, C III, N II, N III, O II, Ne I, Mg II, Si III, Si IV, S II, S III, and Fe III are 0.03, 0.13, 0.03, 0.16, 0.04, 0.02, 0.04, 0.05, 0.13, 0.05, 0.05, and 0.03 dex, respectively.

3.1.2. LTE Analyses

Analysis of the line spectrum was repeated with the TLUSTY LTE models and LTE line analysis. This LTE

analysis uncovers several inconsistencies arising from substantial non-LTE effects on some of the lines. These inconsistencies demand worrying compromises in selecting the atmospheric parameters and, thus, in determining the elemental abundances.

Among the concerns are the fits to the He I and He II line profiles. Observed profiles of He I and the He II 4686 Å lines are shown in Figure 5, with predicted LTE profiles for the LTE atmosphere of $T_{\text{eff}} = 25,300$ K and three different surface gravities. The predicted He I profiles fail to reproduce the observed cores but are acceptable fits to the line wings. Note that the non-LTE profiles provide a satisfactory fit to both the cores and the wings (Figure 2). In LTE, the fit to the He II 4686 Å line requires a much higher surface gravity at a given temperature than other indicators. Figure 6, the LTE counterpart to Figure 3, shows the He I and He II loci, as well as those corresponding to ionization equilibrium.

The loci set by ionization equilibrium for C, N, and Si are almost coincident, and each is only slightly shifted from their non-LTE location in the $T_{\text{eff}}, \log g$ plane. However, the locus set by S II/S III is shifted away from other ionization equilibrium loci because of the large non-LTE effect on the S III lines.

Other species that are subject to appreciable non-LTE effects are not considered when determining the atmospheric

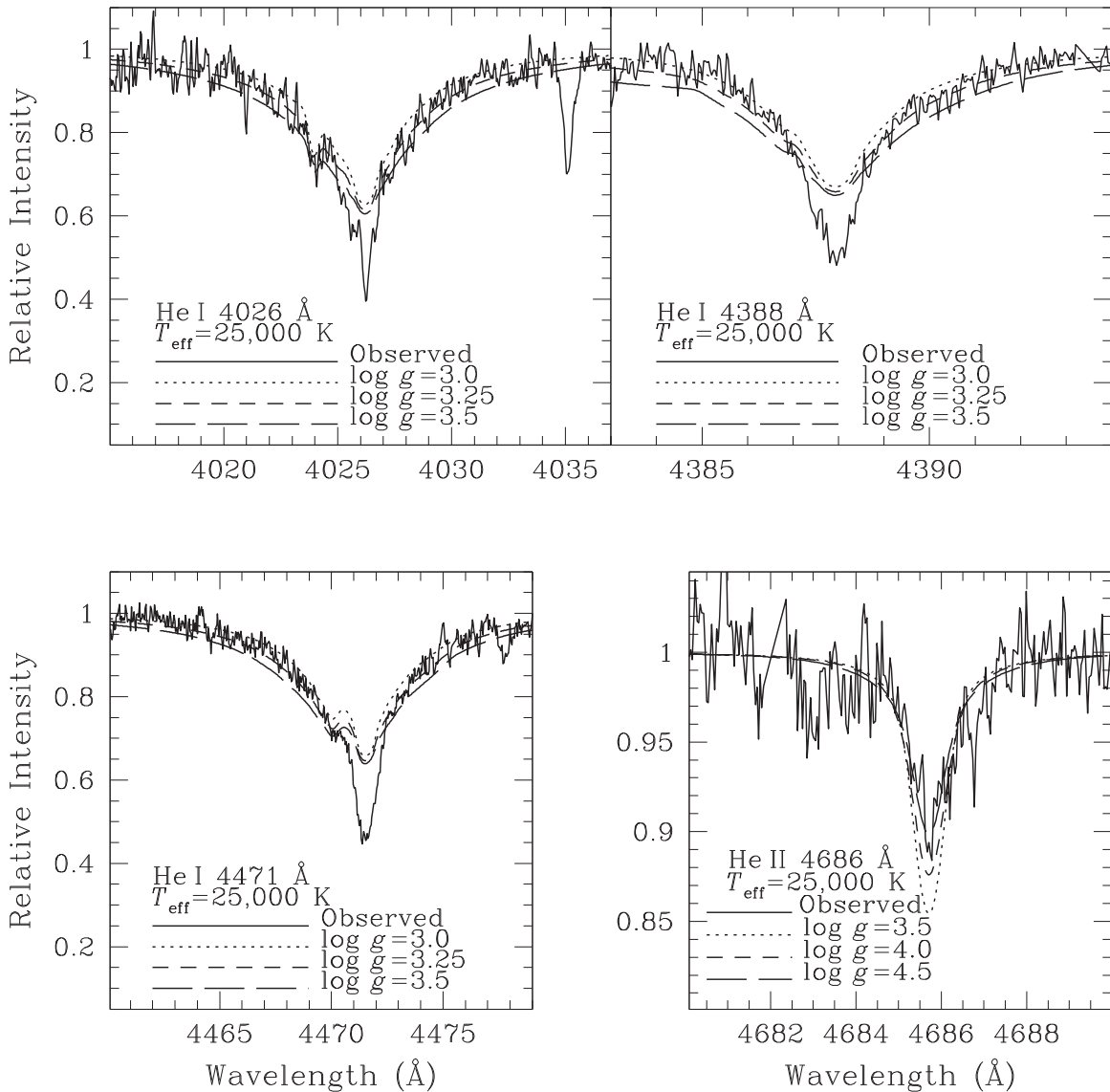


Figure 5. Observed spectrum of V652 Her and theoretical LTE He I and He II line profiles calculated using the LTE model $T_{\text{eff}} = 25,300$ K for three different $\log g$ values—see the key on the figure.

parameters. The species most obviously affected by non-LTE effects is Ne I.

An enthusiast dedicated to LTE analyses with Nelsonian eyesight might adopt the LTE model (see Figure 6) with $T_{\text{eff}} = 25,300 \pm 300$ K, $\log g = 3.25 \pm 0.12$ and a microturbulence of 13 km s^{-1} . The LTE abundances for this adopted LTE TLUSTY model are given in Table 2. The abundance rms errors, due to uncertainty in T_{eff} and $\log g$ from Al III, Si II, P III, and Ar II are 0.05, 0.07, 0.03, and 0.04 dex, respectively. The abundance rms errors for the rest of the species are very similar to those estimated for the appropriate non-LTE model atmosphere. Of course, such errors do not recognize that the choice of the LTE model atmosphere involves compromises.

3.2. HD 144941

3.2.1. Non-LTE Analyses

Essentials of the procedure discussed in Section 3 for V652 Her were adopted for the non-LTE analyses of

HD 144941. A microturbulent velocity $\xi = 10 \text{ km s}^{-1}$ was used as suggested by Harrison & Jeffery (1997). Except for the observed H I and He I lines, all of the lines in the observed spectrum are weak. Of course, the derived abundances from these weak lines are almost independent of the adopted microturbulence.

Fits to the Stark-broadened wings of He I and He II line profiles provide loci in the $(T_{\text{eff}}, \log g)$ plane. Unfortunately, the He II 4686 Å line profile is not detected on our spectrum but the upper limit of its presence provides a limiting locus in the $(T_{\text{eff}}, \log g)$ plane. Figure 7 shows the sample observed profiles with predicted non-LTE profiles for a non-LTE atmosphere of $T_{\text{eff}} = 22,000$ K for three different surface gravities.

The only locus obtained from ionization balance is through sulfur ions S II/S III, but this is based on just one weak S II and two weak S III lines.

Figure 8 shows the loci obtained from the fits to the He I and He II profiles and the ionization balance of S II/S III using model atmospheres computed with small model atoms. These

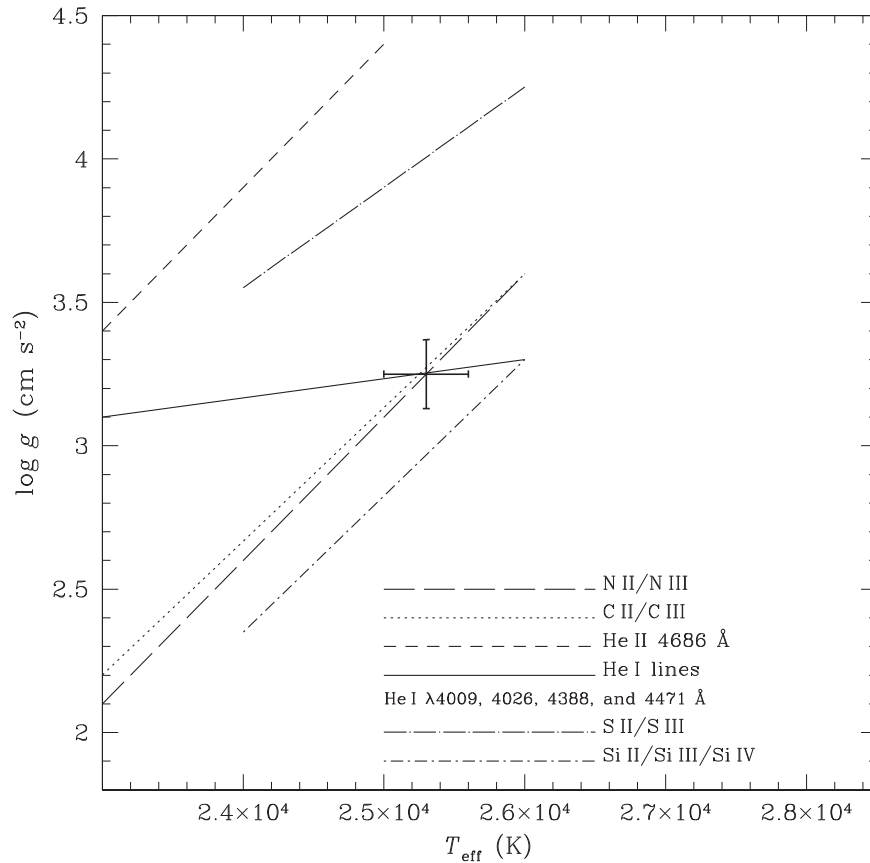


Figure 6. T_{eff} vs. $\log g$ plane for V652 Her. Loci satisfying ionization equilibria are plotted—see the keys on the figure. The loci satisfying optical He I and He II line profiles are shown. The cross shows the adopted LTE model atmosphere parameters.

intersecting loci are used in determining the final model parameters of $T_{\text{eff}} = 22,000 \pm 600$ K and $\log g = 3.45 \pm 0.15$.

Observed profiles of the 4102, 4340, and 4861 Å are shown in Figure 9, with predicted non-LTE profiles for a non-LTE atmosphere of $T_{\text{eff}} = 22,000$ K and $\log g = 3.45$ for three different hydrogen abundances. The line wings are mainly used for this purpose as the predicted profiles show emission in the line-core. Unlike V652 Her, the best fits to the wings are affected by emission in the core, with the intensity of emission increasing from H δ to H β . However, the predicted profiles by Przybilla et al. (2005) match the observations (the wings as well as the core) fairly well. For comparison, observed profiles of the 4102, 4340, and 4861 Å lines for three different H abundances are shown in Figure 10 with predicted non-LTE profiles for a non-LTE atmosphere with the stellar parameters $T_{\text{eff}} = 22,000$ K and $\log g = 4.15$ adopted by Przybilla et al. (2005): $\log \epsilon(\text{H}) = 10.1$ is the non-LTE abundance estimated by Przybilla et al. (2005, 2006).

The non-LTE abundances for the adopted non-LTE TLUSTY model ($T_{\text{eff}}, \log g, \xi$) = (22,000, 3.45, 10.0), computed with small model atoms, are given in Table 3. The abundance rms errors, due to uncertainty in T_{eff} and $\log g$, from C II, N II, O II, Ne I, Mg II, Si III, S II, S III, and Fe III are 0.06, 0.06, 0.05, 0.04, 0.07, 0.06, 0.08, 0.06, and 0.04 dex, respectively.

3.2.2. LTE Analyses

Inconsistencies among atmospheric parameter indicators when using LTE model atmospheres and LTE line analysis techniques may be expected to resemble those inconsistencies

identified as present for V652 Her. The lower abundances of many elements in HD 144941 relative to V652 Her may effect the radiation field in HD 144941's atmosphere, even though opacity at many wavelengths, including the optical region, is dominated by helium.

Observed profiles of the He I and He II 4686 Å line are shown in Figure 11, with predicted LTE profiles for an LTE atmosphere of $T_{\text{eff}} = 21,000$ K and three different surface gravities. As anticipated, the predicted LTE He I profiles for HD 144941 fail to reproduce the observed line-core, but the line wings are well reproduced; the predicted non-LTE He I profiles successfully reproduce the observed core as well as the wings with the adopted non-LTE TLUSTY model (see Figure 7).

The He II 4686 Å line is not positively detected on our spectra. Predicted profiles of this line provide a limiting locus with significantly higher gravities than other indicators, a similar situation occurs for V652 Her (Figure 6).

Figure 12 shows the loci obtained from the fits to the He I and He II profiles and ionization equilibria which are provided by the following pairs of ions: Si II/Si III and S II/S III. The Si locus appears in Figure 12 but not Figure 8 because TLUSTY lacks an adequate model Si⁺ atom. The final compromise LTE model parameters are $T_{\text{eff}} = 21,000 \pm 600$ K and $\log g = 3.35 \pm 0.15$.

LTE abundances for the adopted LTE model are given in Table 3. Observed profiles of the Balmer lines 4102, 4340, and 4861 Å are shown in Figure 13, with predicted LTE profiles for an LTE atmosphere of $T_{\text{eff}} = 21,000$ K and $\log g = 3.35$ for three different hydrogen abundances. The abundance rms

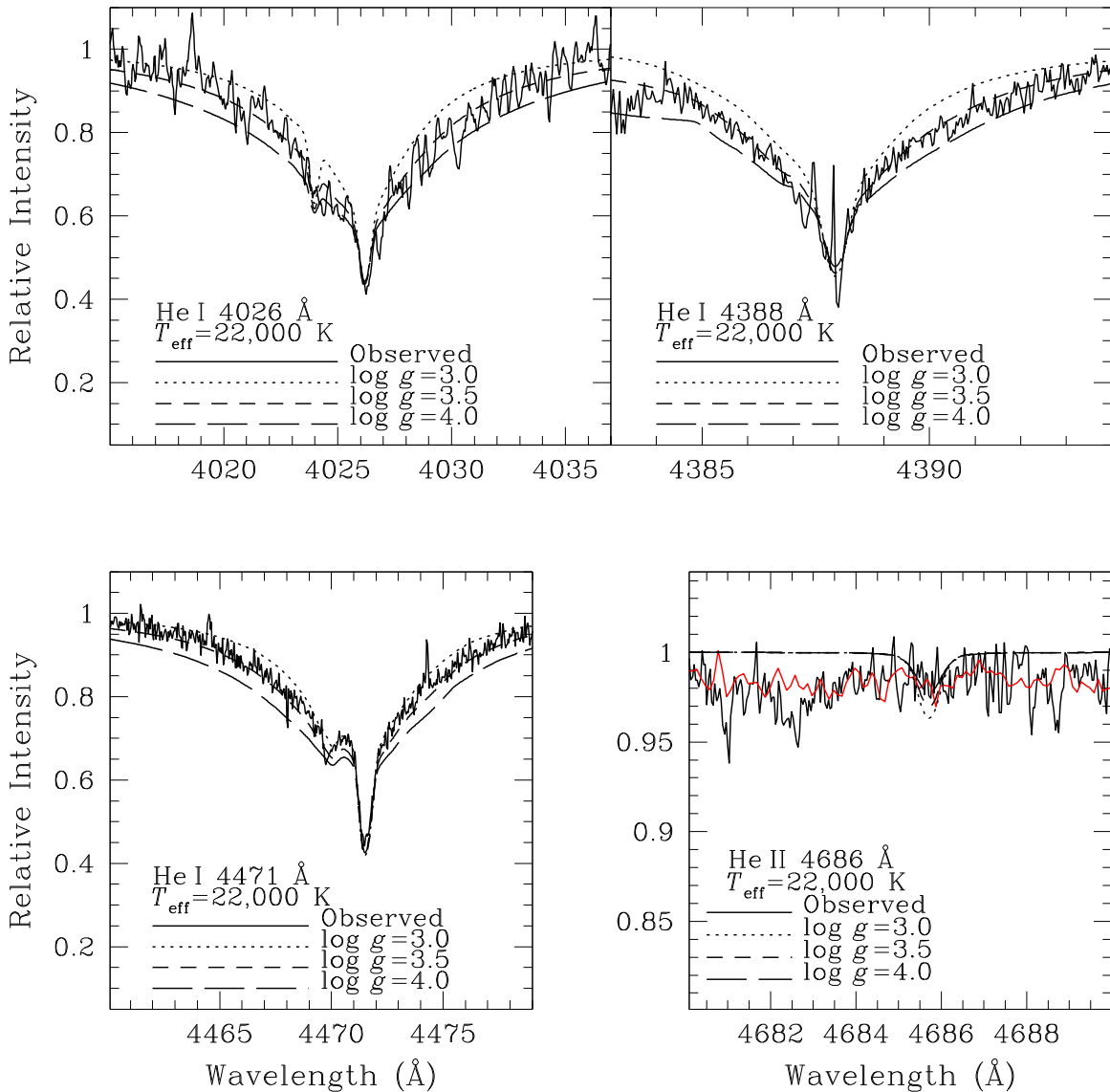


Figure 7. Observed spectrum of HD 144941 and theoretical NLTE He I and He II line profiles calculated using the NLTE model $T_{\text{eff}} = 22,000$ K for three different $\log g$ values—see the key on the figure. The AAT spectrum is shown in red.

errors, due to uncertainty in T_{eff} and $\log g$ from Al III and Si II, are 0.06 and 0.11 dex, respectively. The abundance rms errors for the rest of the species are very similar to those estimated for the appropriate non-LTE model atmosphere. In comparing non-LTE–LTE abundance differences in Table 2 for V652 Her and in Table 3 for HD 144941, it must be noted that the compromise LTE model for V652 Her is 300 K hotter and 0.15 dex greater in $\log g$ than its non-LTE model, but the LTE model for HD 144941 is 1000 K cooler and 0.10 dex lower in $\log g$ than its non-LTE model.

4. Discussion—Chemical Composition

Tables 4 and 5 summarize our derived non-LTE and LTE abundances for V652 Her and HD 144941, respectively. Mean elemental abundances are given for elements represented by more than a single stage of ionization. Composition of the solar photosphere is given in the final column (Asplund et al. 2009).

4.1. V652 Her

Inspection of the abundances for V652 Her offers three pointers toward the star’s history: (i) most obviously, it is H-poor by a factor of about 300, (ii) CNO-cycling was most likely responsible for the conversion of H to He because, as first noted by Jeffery et al. (1999), the star is N-rich and relatively C- and O-poor, and (iii) the overall metallicity of the star is approximately solar, as judged by the abundances of elements from Mg to Fe. Before connecting these points to the star’s evolutionary status, brief remarks are made on the previous LTE abundance analysis of this star.

Jeffery et al. (2001) obtained a time series of optical spectra at a resolving power of 10,000. The results of an LTE abundance analysis when this pulsating star was near maximum radius were given. This LTE atmosphere had parameters $T_{\text{eff}} = 22,000$ K, $\log g = 3.25$, and a microturbulence of 9 km s^{-1} . This model is 3000 K cooler than our LTE model and differs slightly in surface gravity and microturbulence. A direct comparison of LTE abundances (our Table 4 and their

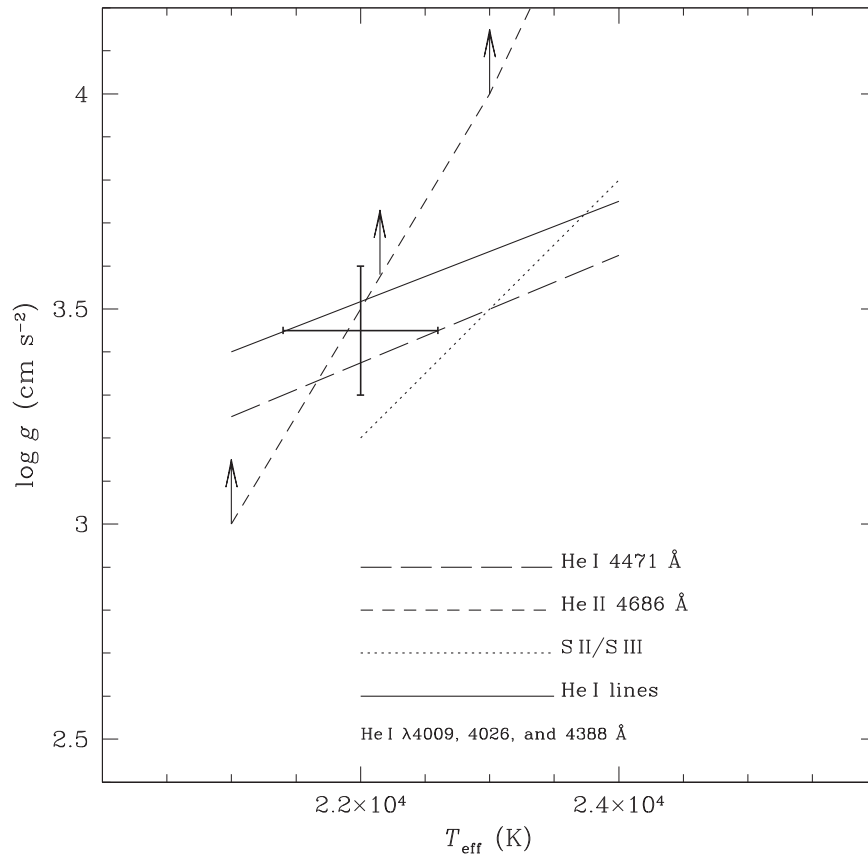


Figure 8. T_{eff} vs. $\log g$ plane for HD 144941. Loci satisfying ionization equilibria are plotted—see the keys on the figure. The loci satisfying optical He I line profiles are shown. The limiting locus for He II is shown by upward arrows. The cross shows the adopted NLTE model atmosphere parameters.

Table 2) gives differences of less than ± 0.3 dex for all of the elements except C, Ne, and P, for which differences in the sense (us–them) are -0.4 , $+0.6$ and -0.9 dex, respectively. Jeffery et al. isolate their P abundance estimate for comment and recommend that “the older value (as provided by Jeffery et al. 1999, p. 498) should be preferred for the present.” This older value for P is within 0.1 dex of our LTE value. When the 1999 values for H to Fe are adopted, the (us–them) differences are within ± 0.3 dex except for S at 0.4 dex. The 1999 LTE model atmospheres corresponded to $T_{\text{eff}} = 24,550 \pm 500$ K, $\log g = 3.68 \pm 0.05$ and a microturbulence 5 km s^{-1} . In short, our and published LTE abundance analyses are in good agreement, but this should be hardly surprising given the similarities of spectra and analytical tools.

Przybilla et al. (2006) provided a hybrid non-LTE analysis (i.e., a non-LTE analysis of absorption lines was made using an LTE model atmosphere) of a selection of lines measured off of the spectrum used by Jeffery et al. (2001). The atmosphere was very similar to that used by Jeffery et al. (2001) and, thus, 3000 K cooler but of similar surface gravity to our chosen non-LTE model atmosphere. The abundances of H, C, N, O, Mg, and S differ in the sense (us–Przybilla) by $+0.3$, -0.4 , $+0.2$, -0.5 , -0.8 and -0.3 dex, respectively. C, Mg, and S were represented by very few lines. With the exception of the Mg abundance from the Mg II 4481 Å feature (the sole Mg indicator), the non-LTE–LTE corrections are within ± 0.2 dex. This independent non-LTE analysis fully confirms the

result that V652 Her’s atmosphere is now highly enriched with CNO-cycled material.

What is new here is the demonstration that the adoption of a set of non-LTE atmospheres and the chosen collection of non-LTE line tools reveals inconsistencies in the indicators previously employed to determine the appropriate atmospheric parameters and corrections to LTE abundances for non-LTE effects, which can for some species (e.g., Ne I) be considerable. At the present time, the non-LTE abundances should be used to discuss the three pointers mentioned in this section’s opening paragraph.

Even if V652 Her is the result of a merger of two He white dwarfs, it is very likely to have retained the metallicity—say, Ne to Fe abundances—of the two stars from which the white dwarfs evolved, with mass loss and mass exchange playing major roles. For the five elements (Ne, Mg, Si, S, and Fe) with non-LTE abundances, the mean difference (V652 Her–Sun) is -0.1 , which suggests a near-solar initial composition. (The differences of -0.5 for Mg and Fe are intriguing.) Thus, V652 Her is a member of the thin disk.

V652 Her’s high N abundance is 0.8 dex above the solar value. This, coupled with the high H deficiency and subsolar values of C and O, point to CNO-cycling as the primary process for the conversion of H to He. The CNO-cycles preserve the total number of C, N, and O nuclei. The non-LTE CNO-sum is 8.78 and the solar sum is 8.92. Almost fortuitously, the expected sum for a mix corresponding to a metal deficiency of -0.1 dex is 8.82!

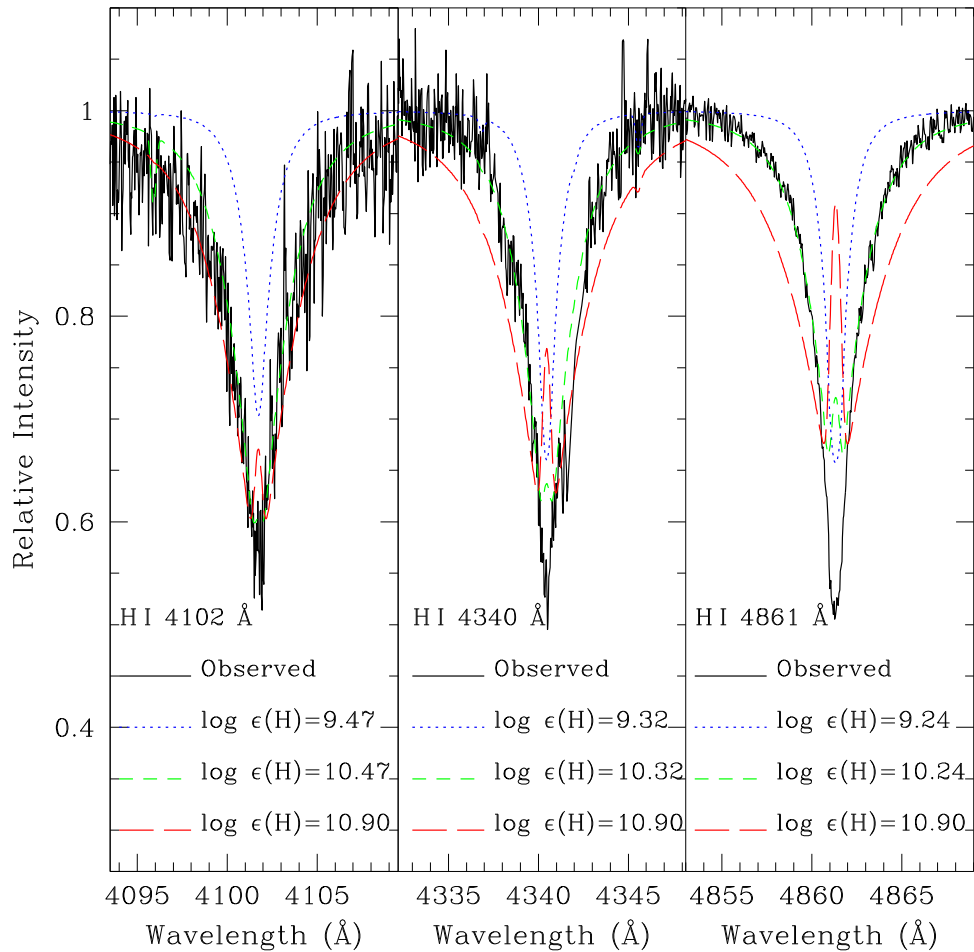


Figure 9. Observed spectrum of HD 144941 and theoretical NLTE H I line profiles calculated using the NLTE model $T_{\text{eff}} = 22,000$ K and $\log g = 3.45$ for three different H abundances—see the key on the figure.

4.2. HD 144941

Comparison of the non-LTE and solar abundances (Table 5) shows a near-uniform difference (star–Sun) for elements from C to Fe. With the exception of Ne and S, the mean difference is -1.6 , with individual values ranging from -1.4 to -1.8 . (The LTE Al abundance gives a difference of -1.4 .) The difference for Fe is ≤ -0.9 . The Fe line at 5156 \AA is present in all three exposures, and clearly seen in Figure 14; however, because this is the sole positive detection and not confirmed by other lines, we assign an upper limit to the Fe abundance. Adopting the Fe abundance from the *IUE* spectra and the LTE analysis by Jeffery & Harrison (1997), the difference is -1.8 , a value consistent with our much higher limit. Their logarithmic Fe abundance of 5.7 ± 0.2 and our non-LTE abundances, except for the α -elements Ne and S, are consistent with the composition of metal-poor stars, residents of the Galactic thick disk or halo, which show α -element enhancements of approximately $+0.3$ for O, Mg, and Si. Moreover, the abundances of C, N, and O are consistent with the difference of -1.6 , and, hence the H deficiency is not obviously attributable to CNO-cycling, as is the case for V652 Her.

As just noted, Ne and S provide striking exceptions to the run of (star–Sun) differences offered by other elements. These elements give differences of -0.7 for Ne and -0.9 for S. There

are no convincing nucleosynthetic reasons for these differences. (Just conceivably, N-rich He-rich material could have been heated and a considerable amount for N burnt to Ne by two successive α -captures. The total initial sum of CNO abundances could have been about 7.3, but the Ne abundance of 7.2 implies a near perfect conversion of CNO to Ne.) The Ne I lines appear to be a secure identification—see Figure 14 for the strongest Ne I line. The primary suspects for the high S abundance are systematic errors associated with the identification of the weak S II and S III lines. The gf -values and non-LTE treatment are less likely sources of errors, as the measured lines are among a larger set used for V652 Her.

Our LTE abundances are in good agreement with the previous LTE analysis of an optical spectrum by Harrison & Jeffery (1997) using the model atmosphere $T_{\text{eff}} = 23,200$ K, $\log g = 3.9$, and a microturbulence of 10 km s^{-1} . The abundance differences (us–them) are within ± 0.25 dex limits. Unfortunately, Harrison & Jeffery did not include Ne and S. Their Fe abundance of 6.4 was lowered to 5.7 by their synthesis of lines in *IUE* spectra (Jeffery & Harrison 1997). Our non-LTE abundances are also in good agreement (except for Mg) with results from the hybrid non-LTE analysis performed by Przybilla et al. (2006): differences (Us–Przybilla) are $+0.3$, 0.0 , -0.3 , -0.4 , and -0.8 dex for H, C, N, O, and Mg, respectively. Our corrections (non-LTE–LTE) are in

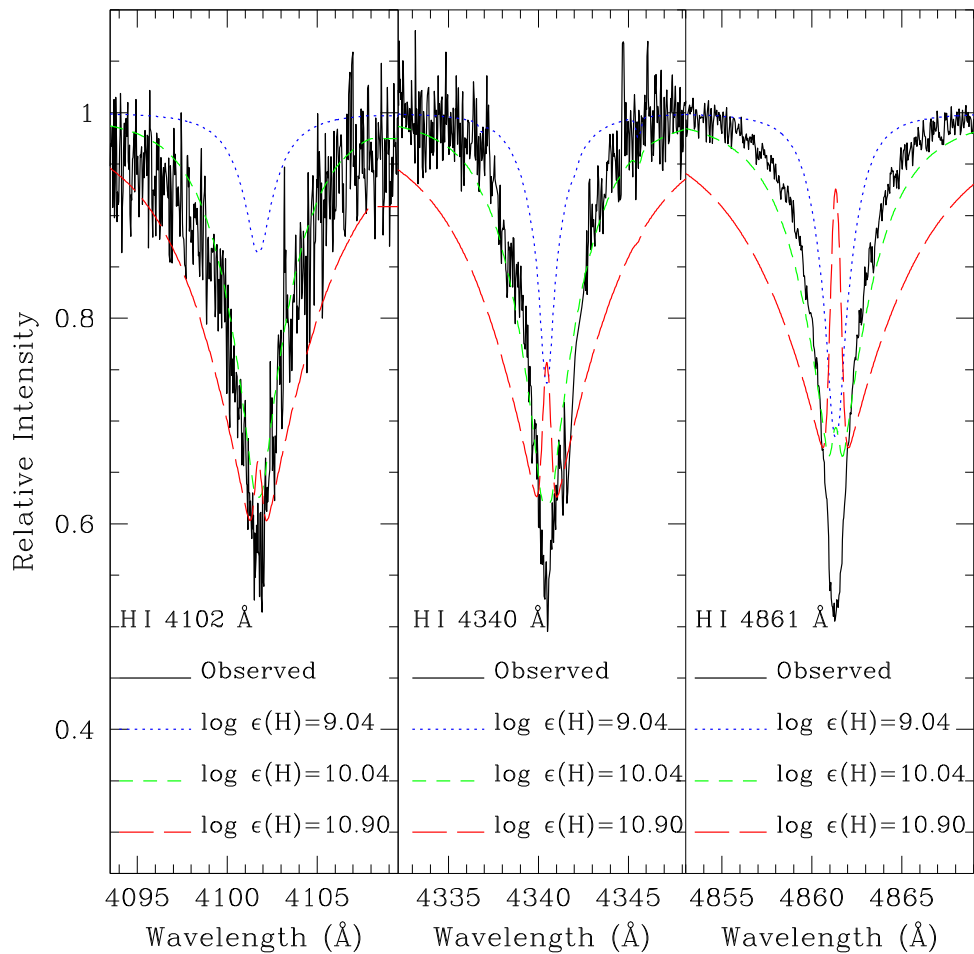


Figure 10. Observed spectrum of HD 144941 and theoretical NLTE H I line profiles calculated using a NLTE model $T_{\text{eff}} = 22,000$ K and $\log g = 4.15$ for three different H abundances—see the key on the figure. These model parameters and the H abundance of 10.04 were adopted based on the estimates of Przybilla et al. (2005).

agreement to within ± 0.15 dex, including for Mg II, with those found by Przybilla et al. (2006). The model atmosphere used by Przybilla et al. (2006) has the same effective temperature but a higher surface gravity ($\log g = 4.15$ rather our 3.45). Przybilla et al. (2006) selected lines from the optical spectrum used by Harrison & Jeffery (1997).

5. Concluding Remarks

A possible origin for extreme He stars such as V652 Her and HD 144941 involves, as noted in the Introduction, the merger of two He white dwarfs. The white dwarfs themselves began life as main sequence stars in a binary system which then experienced two mass exchange and mass loss episodes to form the pair of low-mass He white dwarfs. Emission of gravitational radiation causes the white dwarfs to slowly approach each other. White dwarf binaries that can merge in a Hubble time or less are candidates to account for V652 Her and HD 144941. Zhang & Jeffery (2012) presented evolutionary tracks for the merger of two white dwarfs. Three modes of merger are discussed: slow, fast, and composite. Since their calculations are most extensive for $Z = 0.02$ white dwarfs, V652 Her is discussed first.

In the slow merger (see also Saio & Jeffery 2000), the lower mass white dwarf loses its mass in a few minutes to form a disk around the more massive white dwarf. Accretion from the disk by the surviving white dwarf may last several million years and completes the merger. The composite star is initially a luminous red giant that evolves to become a hot subdwarf before entering the white dwarf cooling track. Along this evolutionary track, the star may appear as an EHe. Zhang & Jeffery’s calculations predict that the surface composition of the merged star (i.e., the EHe) is that of the less massive white dwarf; there is no mixing between the accreted material and the accreting star. The recipe for setting the compositions of the He white dwarfs as described by Zhang & Jeffery proves insensitive to the less massive star’s assumed mass (see Figure 2 from Zhang & Jeffery 2012 for $Z = 0.02$ star). The stars are predicted to be N-rich ($N/C \sim 100$ and $N/O \sim 10$) with $C/He \sim 0.01\%$. This pattern for He, C, N, O, and also Ne matches the observed composition of V652 Her to within a factor of about two (Table 4). (Oddly, the predicted mass fraction of ^{24}Mg is about an order of magnitude higher than observed.) Predicted evolutionary tracks in the ($T_{\text{eff}}, \log g$) plane about the EHe domain are coincident for masses of $0.5\text{--}0.7 M_{\odot}$, with tracks for higher masses occurring at lower surface gravities (see Figure 15 of Zhang & Jeffery 2012). (The

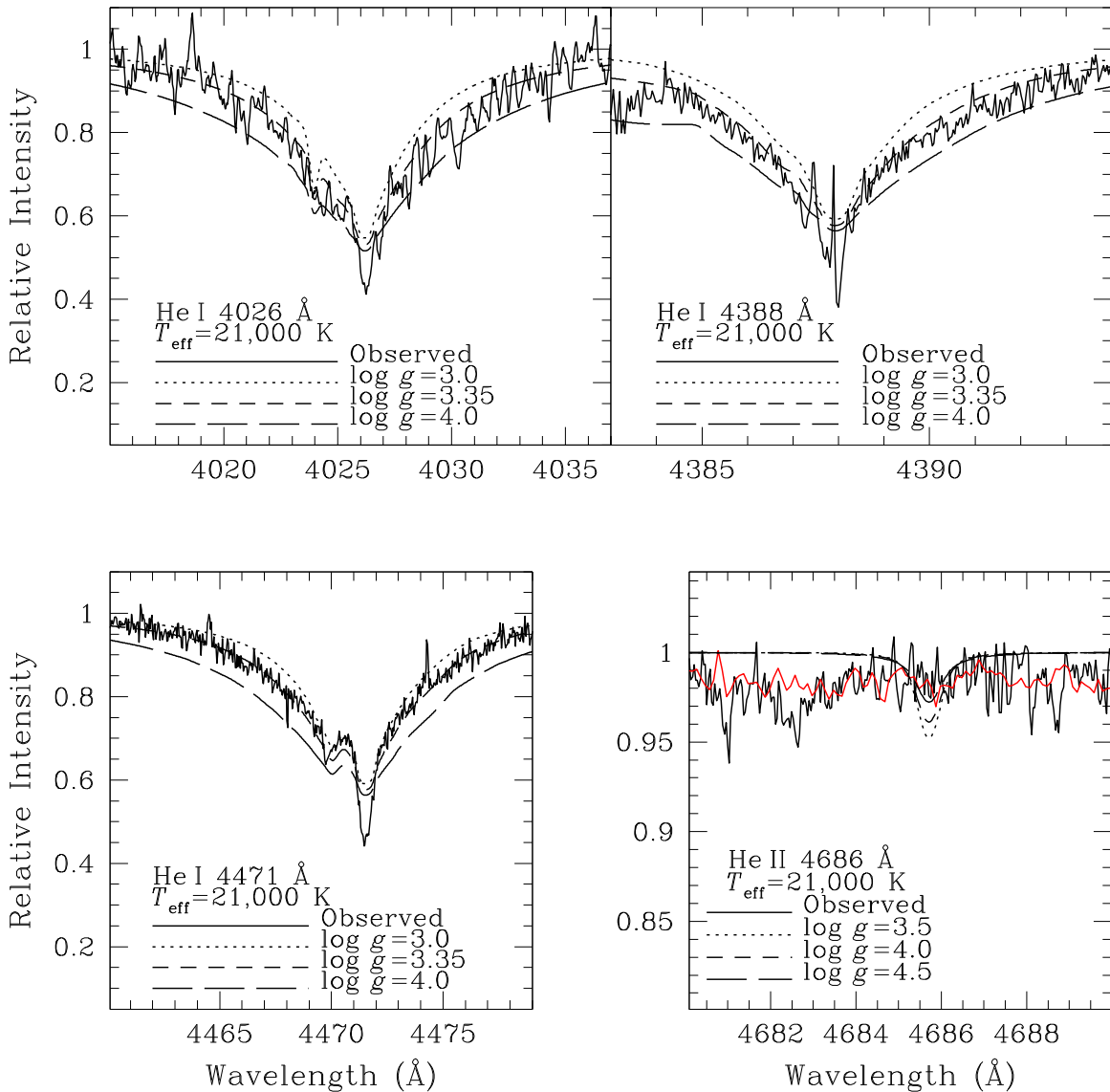


Figure 11. Observed spectrum of HD 144941 and theoretical LTE He I and He II line profiles calculated using the LTE model $T_{\text{eff}} = 21,000$ K for three different $\log g$ values—see the key on the figure. The AAT spectrum is shown in red.

tracks at $T_{\text{eff}} \leq 40,000$ K appear insensitive to the initial composition; $Z = 0.02$ was generally adopted, i.e., slightly supra-solar.) With non-LTE parameters from Table 1, V652 Her falls on the predicted $0.8 M_{\odot}$ track, which is only 0.6 dex lower in $\log g$ than the $0.5\text{--}0.7 M_{\odot}$ tracks. Since Jeffery et al. (2001) estimated V652 Her’s mass at $0.6 \pm 0.2 M_{\odot}$, we consider the observed star as fitting the predicted evolutionary track for a slow merger of two He white dwarfs. This fit is echoed by the correspondence between predicted and observed compositions. In short, V652 Her may be the result of a slow merger of two low-mass He white dwarfs.

In a fast merger, accretion is considered to be complete within a few minutes’ time. In Zhang & Jeffery’s simulations, the envelope resembles a hot corona with carbon produced by He-burning and N destroyed by $^{14}\text{N}(\alpha, \gamma)^{18}\text{O}$; at higher temperatures, α -capture converts the ^{18}O to ^{22}Ne . Burning in a He-shell occurs in flashes. Zhang & Jeffery concluded their description of fast mergers with the remark that “For all the fast

merger models the surface composition is rich in ^{12}C , ^{18}O and ^{22}Ne but there is almost no ^{14}N for models with initial composition of $Z = 0.02$.” (Odintsov 1965, p. 205; of course, it is frustrating that isotopic wavelength shifts for atomic lines with stellar line widths do not permit determinations of the isotopic mix of C, O and Ne.) For slow mergers with $Z = 0.02$, the predicted N/C ratio is about 100 and is independent of the final mass as noted above, but for fast mergers the N/C is predicted to run from 0.01 for a final mass of $0.5 M_{\odot}$ to 10^{-9} for a final mass of $0.8 M_{\odot}$ (see Figure 19 of Zhang & Jeffery 2012). Clearly, V652 Her is not the result of a fast merger.

In the composite model as envisaged by Zhang & Jeffery, the first phase of accretion transfers about half of the mass as a fast merger, with the second half transferred via a disk as in the case of a slow merger. For mergers resulting in a total mass of less than about $0.6 M_{\odot}$ (apparently resulting from roughly equal masses for the two white dwarfs), the surface convection zone is absent and, thus, the surface composition resulting from

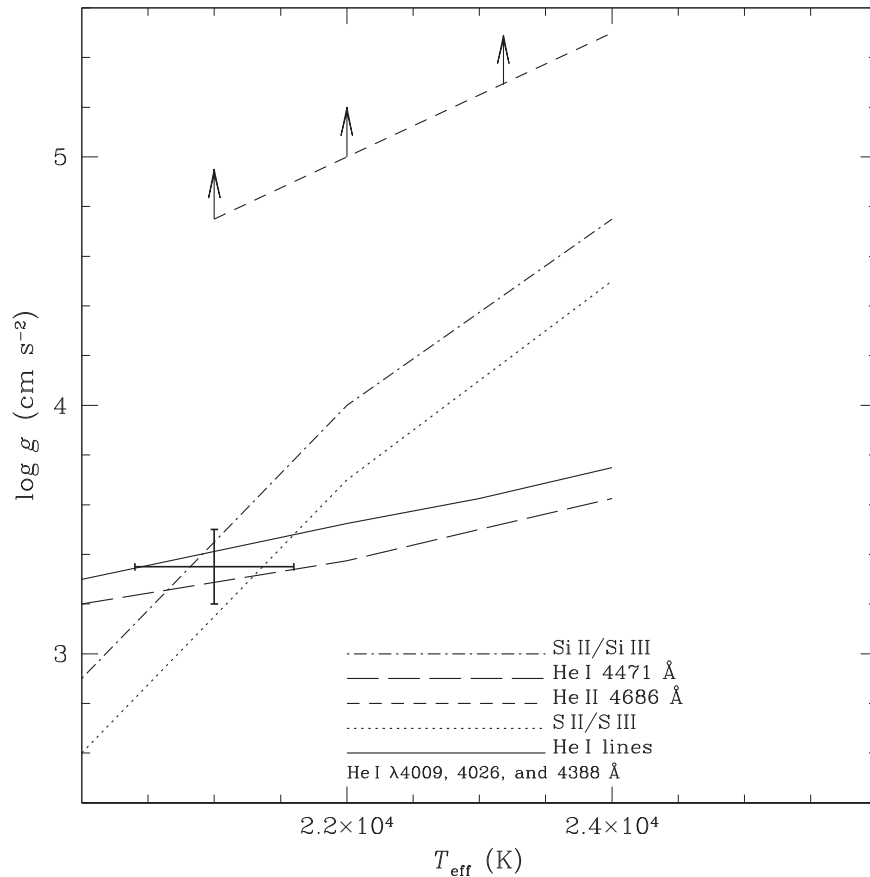


Figure 12. T_{eff} vs. $\log g$ plane for HD 144941. Loci satisfying ionization equilibria are plotted—see the keys on the figure. The loci satisfying optical He I line profiles are shown. The limiting locus for He II is shown by upward arrows. The cross shows the adopted LTE model atmosphere parameters.

accretion from the disk is that of the accreted white dwarf; i.e., the predicted composition is equivalent to that of a slow merger (see Figure 20 from Zhang & Jeffery). At total masses above $0.6 M_{\odot}$, the predicted compositions tend in the direction of those predicted by a fast merger; the N/C ratio is about 0.3 for a mass $0.8 M_{\odot}$, but the prediction for a fast merger is 10^{-11} . V652 Her may have resulted from a composite merger (effectively, a slow merger) with a total mass less than about $0.6 M_{\odot}$.

In brief, V652 Her’s composition and location in the $(T_{\text{eff}}, \log g)$ plane encourage the idea that the star resulted from the merger of two Helium white dwarfs. As modeled by Zhang & Jeffery, the star resulted from a slow or a composite merger with a rather relaxed constraint on the masses of the white dwarfs. A fast merger, as defined by Zhang & Jeffery, leads to a star with N/C less than unity, in sharp conflict with the observed N/C ratio of 50. Significantly, V652 Her’s composition and position in the $(T_{\text{eff}}, \log g)$ plane can be met by a range of slow or composite mergers. In contrast to V652 Her, the picture of a merger of He white dwarfs is not so obviously readily applicable to HD 144941.

An initial impression of HD 144941’s composition (Table 5) is that the C, N, and O are consistent with the initial abundances for a star with $[\text{Fe}/\text{H}]$ of about -1.6 or $Z \sim 0.0004$, but such a consistency surely sits uneasily with the messy conversion of a main sequence star to a highly evolved H-poor star. Moreover, the star’s Ne abundance is about 1 dex greater than anticipated for a normal metal-poor

star. Thus, we have sought possible solutions in Zhang & Jeffery’s paper. It is worthy of note that with respect to the $(T_{\text{eff}}, \log g)$ plane, HD 144941’s non-LTE parameters provide an excellent fit to Zhang & Jeffery’s evolutionary tracks for merging white dwarfs from stars with $Z = 0.001$. Observed and predicted compositions are more difficult to reconcile. For slow mergers at $Z = 0.001$, models predict products with a much lower C/He ratio than observed and a very high N/C ratio (see Figure 20 from Zhang & Jeffery); for example, $\text{N}/\text{C} \sim 200$ but the observed ratio is $\text{N}/\text{C} \sim 0.3$. Fast mergers invert the N/C ratio but are likely to provide an N abundance that declines steeply with increasing total mass, such that a match to HD 144941 will be found only for a narrow range of masses. A composite merger may match the observed He, C, and N abundances with adjustments to Zhang & Jeffery’s recipe for this merger process. The introduction of a period of fast merging is expected to increase the Ne (as ^{22}Ne) abundance and so possibly match the observed Ne abundance. (An episode of fast merging may also provide abundant ^{18}O .) Expansion of the parameter space considered by Zhang & Jeffery is highly desirable.

Our abundance analysis shows that the use of non-LTE effects in the construction of model atmospheres and analyses of absorption lines for He-rich warm stars leads to significant changes in the defining atmospheric abundances, and in certain elemental abundances relative to the assumption of LTE for model atmospheres and abundance analysis. Judging by our determinations of composition and location in the $(T_{\text{eff}}, \log g)$

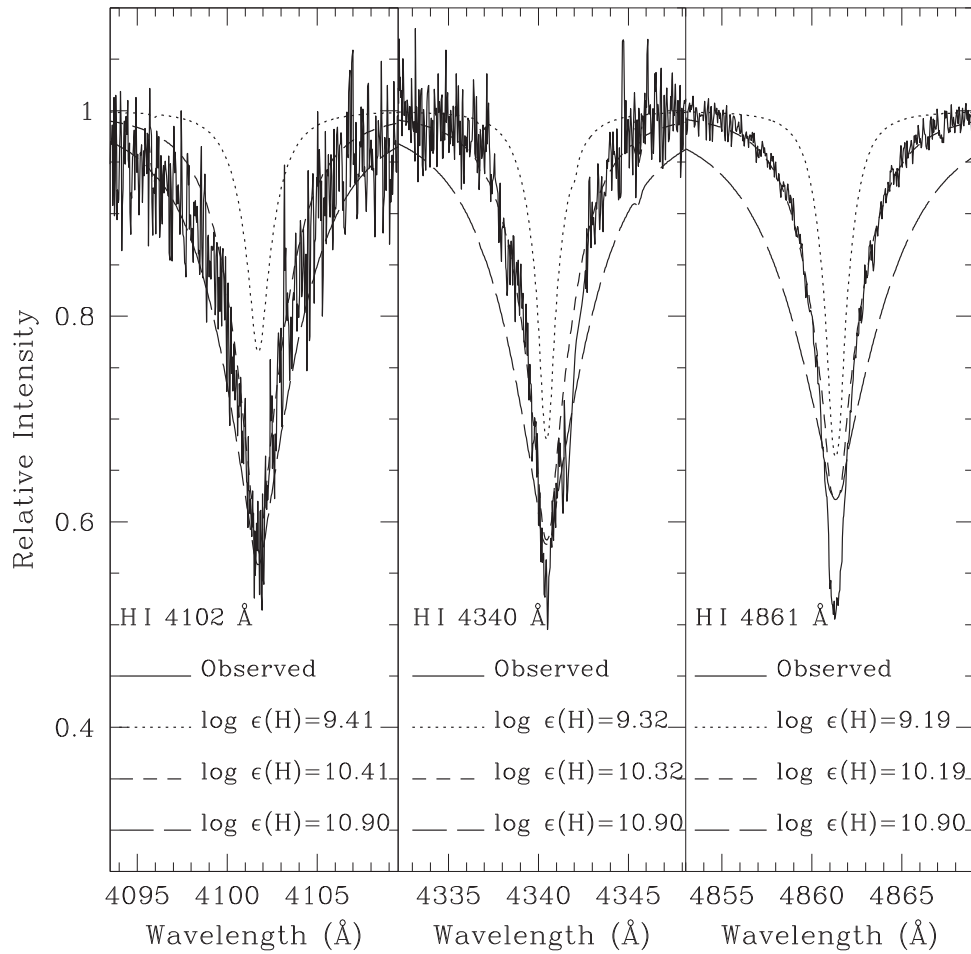


Figure 13. Observed spectrum of HD 144941 and theoretical LTE H I line profiles calculated using the LTE model $T_{\text{eff}} = 21,000$ K and $\log g = 3.35$ for three different H abundances—see the key on the figure.

Table 4
Summary of V652 Her’s Photospheric Abundances

Element	Non-LTE	LTE	Sun ^a
H	9.5	9.7	12.0
He	11.5	11.5	10.9
C	7.0	6.9	8.4
N	8.7	8.9	7.8
O	7.6	7.6	8.7
Ne	8.1	8.6	7.9
Mg	7.1	7.5	7.6
Al	...	6.4	6.5
Si	7.4	7.4	7.5
P	...	5.5	5.4
S	7.4	7.2	7.1
Ar	...	6.9	6.4
Fe	7.1	7.3	7.5

Note.
^a Asplund et al. (2009).

Table 5
Summary of HD 144941’s Photospheric Abundances

Element	Non-LTE	LTE	Sun ^a
H	10.4	10.4	12.0
He	11.5	11.5	10.9
C	6.9	6.6	8.4
N	6.4	6.7	7.8
O	7.1	7.0	8.7
Ne	7.2	7.5	7.9
Mg	5.8	5.9	7.6
Al	...	5.1	6.5
Si	6.0	6.0	7.5
S	6.2	6.0	7.1
Fe	≤6.6	≤6.2	7.5

Note.
^a Asplund et al. (2009).

plane, V652 Her is likely to have resulted from the merger of two helium white dwarfs. HD 144941’s location in the ($T_{\text{eff}}, \log g$) plane is similarly consistent with the merger hypothesis. Its composition may also be consistent with formation through a merger, but additional theoretical

predictions seem required. These conclusions are based on Zhang & Jeffery’s bold and exploratory calculations of the merging process. Our analyses will perhaps not only encourage refinements to the study of white dwarf mergers but also a search for additional EHe stars with the very low C/He ratio that is a characteristic feature of V652 Her and HD 144941.

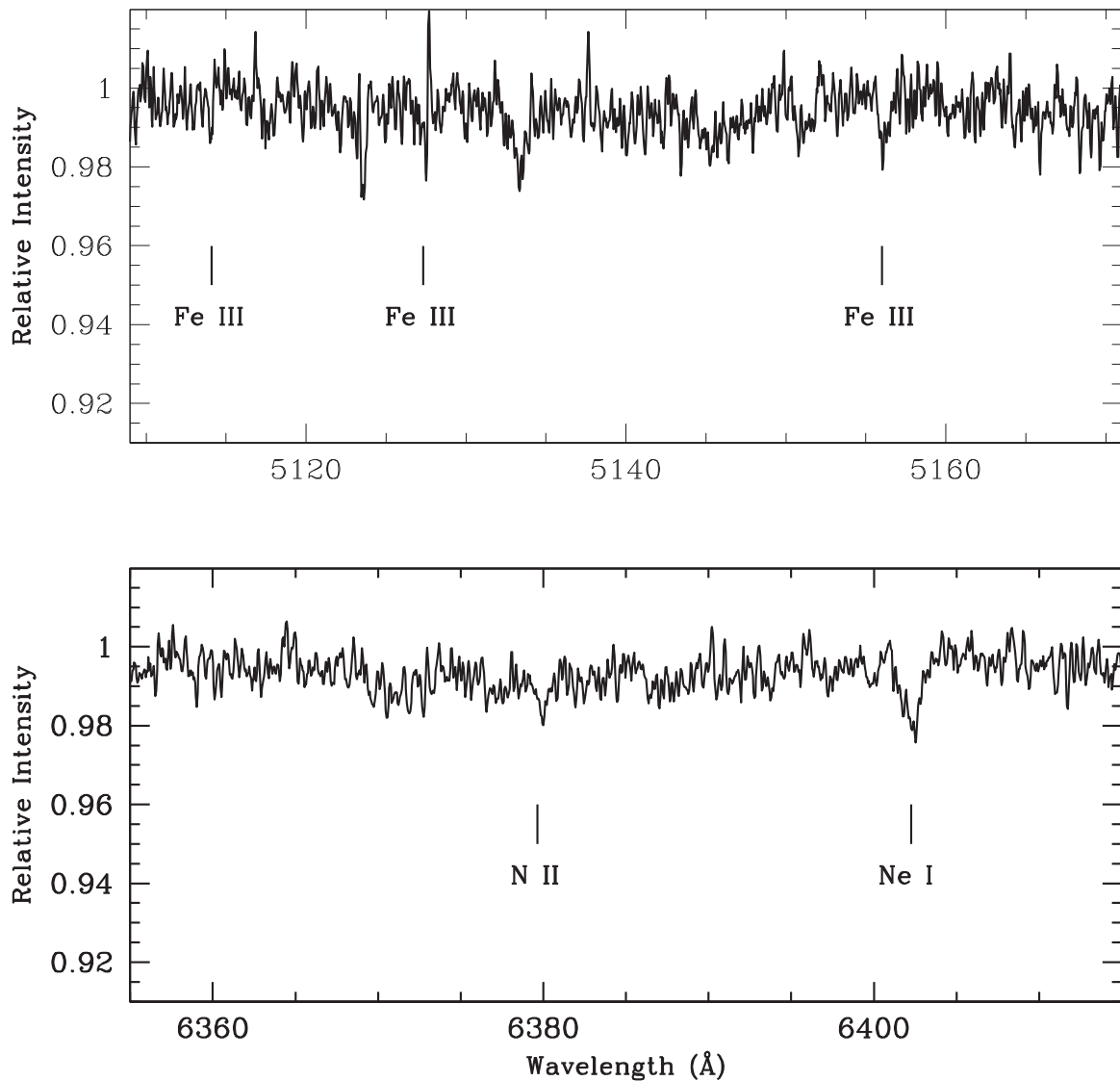




Figure 14. Two sample spectral regions are shown for HD 144941. The positions of the key lines are marked in particular Ne I and Fe III lines; these lines are the strongest among the other measured Ne I and Fe III lines, respectively.

Quite fortuitously, after the submission of this paper, Jeffery (2017) reported the discovery of a third EHe star with a low C/He ($=0.0023\%$) ratio. According to the LTE abundance analysis by Jeffery (2017), the star *GALEX* J184559.8-413827 has a subsolar (-0.4) metallicity with C, N, and O abundances similar to that of V652 Her; i.e., the atmosphere of the new discovery is rich in CNO-cycled material. Our abundance analyses of V652 Her show that a non-LTE reanalysis of J184559.8-413827 will not alter this conclusion.

We thank Simon Jeffery and Mike Montgomery for helpful email exchanges. We also thank Ivan Hubeny for helping us use the TLUSTY and SYNSPEC codes. We would like to thank the anonymous referee for constructive comments. D.L. acknowledges the support of the Robert A. Welch Foundation of Houston, Texas through grant F-634.

ORCID iDs

Gajendra Pandey  <https://orcid.org/0000-0001-5812-1516>
David L. Lambert  <https://orcid.org/0000-0003-1814-3379>

References

- Asplund, M., Grevesse, N., Sauval, A. J., & Scott, P. 2009, *ARA&A*, **47**, 481
 Barnard, A. J., Cooper, J., & Smith, E. W. 1974, *QJRT*, **14**, 1025
 Harrison, P. M., & Jeffery, C. S. 1997, *A&A*, **323**, 177
 Hill, P. W., Kilkeny, D., Schoenberner, D., & Walker, H. J. 1981, *MNRAS*, **197**, 81
 Hubeny, I. 1988, *CoPhC*, **52**, 103
 Hubeny, I., & Lanz, T. 1995, *ApJ*, **439**, 875
 Hubeny, I., & Lanz, T. 2011, Synspec: General Spectrum Synthesis Program, Astrophysics Source Code Library, ascl:1109.022
 Hubeny, I., & Lanz, T. 2017, arXiv:1706.01859
 Hubeny, I., Lanz, T., & Jeffery, C. S. 1994, in Newsletter on Analysis of Astronomical Spectra 20, ed. C. S. Jeffery (CCP7; St. Andrews: St. Andrews Univ.), 30
 Jeffery, C. S. 2008, in ASP Conf. Ser. 391, Hydrogen-Deficient Stars, ed. A. Werner & T. Rauch (San Francisco, CA: ASP), 53
 Jeffery, C. S. 2017, *MNRAS*, **470**, 3557
 Jeffery, C. S., & Harrison, P. M. 1997, *A&A*, **323**, 393
 Jeffery, C. S., Hill, P. W., & Heber, U. 1999, *A&A*, **346**, 491
 Jeffery, C. S., Woolf, V. M., & Pollacco, D. L. 2001, *A&A*, **376**, 497
 Landolt, A. U. 1975, *ApJ*, **196**, 789
 Moore, C. E. 1972, NSRDS-NBS, **40**, 1
 Moore, C. E. 1993, Tables of Spectra of Hydrogen, Carbon, Nitrogen, and Oxygen Atoms and Ions (Boca Raton, FL: CRC Press)

- Pandey, G., Kameswara Rao, N., Jeffery, C. S., & Lambert, D. L. 2014, *ApJ*, **793**, 76
- Pandey, G., Kameswara Rao, N., Lambert, D. L., Jeffery, C. S., & Asplund, M. 2001, *MNRAS*, **324**, 937
- Pandey, G., & Lambert, D. L. 2011, *ApJ*, **727**, 122
- Przybilla, N., Butler, K., Heber, U., & Jeffery, C. S. 2005, *A&A*, **443**, L25
- Przybilla, N., Nieva, M. F., Heber, U., & Jeffery, C. S. 2006, *BaltA*, **15**, 163
- Saio, H., & Jeffery, C. S. 2000, *MNRAS*, **313**, 671
- Shamey, L. J. 1969, PhD thesis, University of Colorado at Boulder
- Tull, R. G., MacQueen, P. J., Sneden, C., & Lambert, D. L. 1995, *PASP*, **107**, 251
- Vidal, C. R., Cooper, J., & Smith, E. W. 1973, *ApJS*, **25**, 37
- Zhang, X., & Jeffery, C. S. 2012, *MNRAS*, **419**, 452